Development of the kinetically and atomically balanced generalized pseudospectral method

Li Guang Jiao [*] and Yu Ying He
College of Physics, Jilin University, Changchun 130012, People's Republic of China

Aihua Liu [†]
Institute of Atomic and Molecular Physics, Jilin University, Changchun 130012, People's Republic of China

Yong Zhi Zhang
College of Physical Science and Technology, Heilongjiang University, Harbin 150080, People's Republic of China

Yew Kam Ho
Institute of Atomic and Molecular Sciences, Academia Sinica, Taipei 10617, Taiwan

(Received 1 December 2020; revised 20 March 2021; accepted 19 July 2021; published 2 August 2021)

The kinetically and atomically balanced conditions have been extensively used in various basis-set expansion methods to remove the nonphysical spurious states appearing in the numerical calculation of the Dirac equation; however, they are generally not applicable for methods in discrete variable representation. In this paper we show that these conditions can be conveniently introduced into the generalized pseudospectral (GPS) method. Four types of balanced condition, the mono kinetic balance (MKB), dual kinetic balance, mono atomic balance (MAB), and dual atomic balance, are incorporated into the GPS method to eliminate the spurious states. Numerical calculations for a variety of bound states of H-like ions in point-charge models are compared with the analytical solutions to demonstrate the accuracy and efficiency of the developed methods. The application to highly charged ions with extended nuclear models is performed to show the flexibility of the balanced GPS methods in practical atomic structure calculations. It is concluded that the MAB-GPS and MKB-GPS methods, which are both free of any spurious states, show better performance and simpler implementation than the others in solving the Dirac equation with the potential in point-charge and extended nuclear models, respectively. The balanced GPS methods developed in this paper provide a useful tool for accurately solving the one-electron Dirac equation and efficiently constructing the multielectron relativistic wave functions.

DOI: 10.1103/PhysRevA.104.022801

I. INTRODUCTION

Accurate solution of the time-independent and time-dependent Dirac equation has become of great importance in the last few decades with fast development of high-precision measurements in atomic and molecular systems and new advances in light source technology and strong laser-matter interaction. Precise treatment of the relativistic one-electron system not only provides an ideal prototype to test the accuracy of various numerical methods, but also serves as the foundation in investigating the structure and dynamics of complex systems; e.g., in the multiconfiguration Dirac-Fock or relativistic configuration-interaction framework the multielectron system wave functions are usually constructed in terms of one-electron Dirac spinors [1–5], and in strong laser-atom interactions the single active electron approximation is commonly used so that one only needs to solve the one-electron time-dependent Dirac equation [6–10]. Unlike the nonrelativistic Schrödinger equation, the spectrum of the Dirac equation does not have a lower bound due to the existence of the Dirac sea. Variational calculation of the radial Dirac equation generally encounters the problem of spurious states when one uses a sequence of finite-dimensional spaces (or basis sets) to approximate the spectrum of the Dirac Hamiltonian in an infinite-dimensional Hilbert space [11,12].

Numerous theoretical approaches including the basis-set expansion and discrete variable representation (DVR) methods, which are well suited for solving the Schrödinger equation, have been developed to work in the relativistic case. In earlier research works, the nonphysical spurious states are usually disregarded in practical calculation of atomic properties. However, as mentioned by many authors [13–15], the existence of spurious states would not only worsen the convergence of basis-set expansions or discrete variable calculations, but also lead to large errors in the prediction of subtle atomic properties such as the self-energy correction in QED calculations [13], the hyperfine interactions [14], and the parity-non-conserving amplitudes [15]. The removal of spurious states in the very beginning of the calculation of the Dirac equation would be the preferred choice.

The basis-set expansion method attracts the majority of interest in the numerical solution of the Dirac equation on

[*] lgjiao@jlu.edu.cn
[†] aihualiu@jlu.edu.cn

account of its fundamental role in the construction of multielectron wave functions. The earlier work of Drake and Goldman [16] has generalized the Slater- and Laguerre-type functions for use in the discrete basis-set expansion calculations. Grant and coworkers [1,17–19] have explicitly incorporated the kinetically balanced condition into the basis sets in terms of Coulomb Sturmians, Slater-type orbitals, and Gaussian functions, and the new basis functions are referred to as *L*-, *S*-, and *G*-spinors, respectively. These basis sets build the foundation of the well-known relativistic atomic structure package GRASP [20]. The B-spline functions also attracted considerable attention in the Rayleigh-Ritz and Galerkin approximations of the Dirac equation. Johnson and coworkers [21,22] have introduced additional boundary constraints (known as the Notre Dame or MIT bag model) at the outer boundary of B-splines to move the spurious eigenvalue onto the top of the spectrum. The spurious solution is far away from the physical spectrum so that it can be manually removed from numerical calculations. Such a method has been successfully used by several authors in the investigation of relativistic atomic polarizabilities [23]. A revealing analysis of the shift of the spurious state is also available in Beloy and Derevianko [14]. The kinetically balanced B-splines, which to some extent are similar to the *L*-, *S*-, and *G*-spinors developed by Grant and coworkers [17–19], have been experimented on by Igarashi [24] and Shabaev *et al.* [13], where the former author implied the kinetic matching constraint solely on the lower component of basis functions, while the latter authors proposed the use of the dual kinetically balanced condition on both the upper and lower components. Further discussions on the prosperity of the kinetically balanced methods and their computational details are available in Refs. [14,15,25]. On the other side, a number of techniques have also been developed for different DVR methods to overcome the spurious problem. For the finite-difference method, Salomonson and Öster [26] have shown that the spurious states introduced by the discrete representation of the first-order derivative can be avoided by defining the upper and lower components of the radial wave function on alternating lattice sites. However, careful attention must be paid on the boundary conditions due to the fact that one needs to know the wave functions in a few points outside the lattice. It is also worth noting that such a technique has a similar effect to the B-spline method with different polynomial orders [15] as a way of avoiding spurious solutions. An alternative method by introducing an extra Wilson term into the Hamiltonian seems to be useful in separating the physical states from spurious solutions and improving the accuracy of finite-difference method [27]. The finite-element method also suffers from the appearance of spurious solutions in the positive-energy spectrum [28], and such problem was not solved until the streamline upwind Petrov-Galerkin approximation developed by Almanasreh *et al.* [29,30] was applied to perform the finite-element computation. The well-developed mapped Fourier grid method, when applied to the Dirac equation, is also accompanied by the occurrence of spurious states [31,32] and this problem has not yet been fully solved. It is worth mentioning that the Lagrange-mesh method [33,34] has been successfully extended to solve the Dirac equation, while it is claimed by the authors that the spurious states may exist in some special cases when a limited number of grid points is used [33]. From the brief overview one may find that the removal of spurious states in DVR methods is much more involved than the basis-set expansion methods, e.g., the kinetic balance technique which has been extensively used in the latter case seems to be inapplicable to the DVR methods.

In the past few years, the pseudospectral (or semispectral) method [35,36] has attracted considerable interest in atomic, molecular, and nuclear physics on account of its prominent merit as a global approach in DVR. The pseudospectral method possesses exponential convergence with respect to the number of discrete points which is much faster than the finite-difference and finite-element methods. Compared to the basis-set expansion methods where one has to calculate the potential matrix elements, which is generally the most time-consuming part, the implementation of the pseudospectral method is very straightforward and nearly has no restrictions on the exact form of interaction potentials. The generalized pseudospectral (GPS) method was first developed by Yao and Chu [37] to calculate the one-electron bound and resonance states in both the Schrödinger and Dirac equations, although in the latter situation spurious solutions still exist. Since then, great success of the nonrelativistic GPS method as a powerful tool to solve the time-independent and time-dependent problems has been made by many authors in investigating the multiphoton and above-threshold ionization and high-order harmonic generation in intense laser-atom and molecule interactions [38–42], the bound properties of plasma screened and spatially confined atoms [43–49], and the multiply excited resonance states of multielectron systems [50–54]. The application of GPS method to the relativistic calculations, in contrast, is rather limited and the pollution of spurious states to the physical eigenstates in such a scheme has not yet been solved [37]. An advancement of the GPS method was recently made by Telnov *et al.* [55] in the investigation of multiphoton ionization of one-electron relativistic diatomic quasimolecules in strong laser fields. By formulating the four-component Dirac equation in prolate spheroidal coordinates, it is reported that the spurious states do not show up in the numerical solutions of the time-independent and time-dependent Dirac equations. The most recent development by these authors applied the dual kinetic balance approach into the GPS method in cylindrical coordinates [56], and the proposed method shows great successes in the study of relativistic ionization dynamics of H-like ions in strong laser fields.

In this paper, we would take a systematic research on the development of kinetically and atomically balanced GPS methods in solving the time-independent relativistic Dirac equation, and demonstrate the robustness of these methods in removing the spurious states and improving the convergence of calculation. The successful development of the relativistic GPS methods to be free of any spurious states, combined with the multielectron approximations and efficient time propagation techniques, would provide a useful tool for accurately studying the structure and response of atomic and molecular systems in the relativistic regime. This paper is organized as follows. In Sec. II, we first revisit the Dirac equation and the original GPS method, and then present in detail the theoretical effort in introducing the mono and dual, kinetically and atomically balanced conditions into the GPS method. Thorough tests on the four types of balanced GPS methods are included

in Sec. III by comparing with the analytical solutions of H-like atoms with point-charge nuclei and applying them to the highly charged ions with extended nucleus models. We finally give our conclusions in Sec. IV. Atomic units (a.u.) $\hbar = m_e = e = 1$ and the speed of light $c = 1/\alpha = 137.035\,999\,084$ [57] are used throughout this paper unless otherwise specified.

II. THEORETICAL METHOD

A. Radial Dirac equation

The relativistic Dirac equation for the one-electron system reads

$$H_D\psi(\boldsymbol{r}) = E\psi(\boldsymbol{r}), \tag{1}$$

where the eigenenergy E includes both the electronic state energy ε and the rest energy c^2,

$$E = \varepsilon + c^2, \tag{2}$$

and H_D is the Dirac Hamiltonian,

$$H_D = c\boldsymbol{\alpha}\cdot\boldsymbol{p} + \beta c^2 + V(\boldsymbol{r}), \tag{3}$$

in which $\boldsymbol{p}$ is the momentum operator, and $\boldsymbol{\alpha}$ and β are the traditional 4×4 matrices of Dirac operators [58]. In this paper, we restrict our calculations on the spherically symmetrical potential, i.e., $V(\boldsymbol{r}) = V(r)$. Then the system eigenstates take the form

$$\psi_{n\kappa m}(\boldsymbol{r}) = \frac{1}{r}\begin{pmatrix} P_{n\kappa}(r)\chi_{\kappa m}(\theta,\varphi) \\ iQ_{n\kappa}(r)\chi_{-\kappa m}(\theta,\varphi)\end{pmatrix}, \tag{4}$$

where $P_{n\kappa}(r)$ and $Q_{n\kappa}(r)$ are the large and small components of the radial wave function, respectively. The angular parts $\chi_{\pm\kappa m}(\theta,\varphi)$ are eigenstates of $\boldsymbol{L}^2$, $\boldsymbol{S}^2$, $\boldsymbol{J}^2$, and J_z with the eigenvalues being $l(l+1)$, $3/4$, $j(j+1)$, and m. The Dirac quantum number κ is connected with the total and orbital angular momenta j and l by

$$\kappa = l(l+1) - j(j+1) - 1/4. \tag{5}$$

By substituting Eqs. (3) and (4) into Eq. (1) and separating the angular parts from radial ones, we get the coupled radial Dirac equations in the form

$$\begin{pmatrix} V(r)+c^2 & -c\left(\frac{d}{dr}-\frac{\kappa}{r}\right) \\ c\left(\frac{d}{dr}+\frac{\kappa}{r}\right) & V(r)-c^2\end{pmatrix}\begin{pmatrix} P_{n\kappa}(r) \\ Q_{n\kappa}(r)\end{pmatrix} = E\begin{pmatrix} P_{n\kappa}(r) \\ Q_{n\kappa}(r)\end{pmatrix}. \tag{6}$$

The radial Dirac spinors $P(r)$ and $Q(r)$ for bound states are normalized by

$$\int_0^\infty \left[P_{n\kappa}^2(r) + Q_{n\kappa}^2(r)\right]dr = 1. \tag{7}$$

It is well known that for the H-like ions with point-charge nuclei where the potential simplifies to

$$V(r) = -\frac{Z}{r}, \tag{8}$$

Eq. (6) can be solved analytically with eigenenergies being

$$E_{n\kappa} = c^2\left[1 + \frac{(\alpha Z)^2}{(n-|\kappa|+\gamma)^2}\right]^{-1/2}, \tag{9}$$

where

$$\gamma = \sqrt{\kappa^2 - \frac{Z^2}{c^2}}. \tag{10}$$

The corresponding eigenstates are also analytically available in the literature [58]. It is worth noting that near $r = 0$ the radial Dirac spinors behave as [19]

$$P_{n\kappa}(r) \xrightarrow{r\to 0} r^\gamma, \quad Q_{n\kappa}(r) \xrightarrow{r\to 0} \frac{c(\kappa+\gamma)}{Z}r^\gamma, \tag{11}$$

which represent the vanishing of radial Dirac spinors at the origin. For large r and assuming $V(r)\to 0$ as $r\to\infty$, they decrease exponentially [1]:

$$P_{n\kappa}(r) \xrightarrow{r\to\infty} e^{-\lambda r}, \quad Q_{n\kappa}(r) \xrightarrow{r\to\infty} \sqrt{\frac{c^2-E}{c^2+E}}e^{-\lambda r}, \tag{12}$$

where

$$\lambda = \sqrt{c^2 - \frac{E^2}{c^2}}. \tag{13}$$

B. Generalized pseudospectral method

The generalized pseudospectral was first introduced by Yao and Chu [37] to efficiently solve the radial Schrödinger and Dirac equations in discrete variable representation. The semi-infinite domain $[0,\infty]$ of radial variable r is mapped onto the finite interval $[-1,1]$ through an algebraic mapping function

$$r = f(x) = L\frac{1+x}{1-x}, \tag{14}$$

in which L is the mapping parameter that adjusts the discretization of r with fixed x. The radial wave function is then transformed by

$$\phi(x) = \sqrt{f'(x)}\psi(r), \tag{15}$$

where in the Dirac equation the radial wave functions have two components:

$$\phi(x) = \begin{pmatrix} p(x) \\ q(x)\end{pmatrix}, \quad \psi(r) = \begin{pmatrix} P(r) \\ Q(r)\end{pmatrix}. \tag{16}$$

The normalization condition shown in Eq. (7) simplifies to

$$\int_{-1}^{1}[p^2(x) + q^2(x)]dx = 1. \tag{17}$$

After several algebraic manipulations, one gets the new coupled first-order differential equation with respect to the variable x [59]:

$$h_D(x)\phi(x) = E\phi(x), \tag{18}$$

where

$$h_D(x) = \begin{pmatrix} V(f(x))+c^2 & c\frac{\kappa}{f(x)} \\ c\frac{\kappa}{f(x)} & V(f(x))-c^2\end{pmatrix} + \begin{pmatrix} 0 & -c \\ c & 0\end{pmatrix}\frac{1}{\sqrt{f'(x)}}\frac{d}{dx}\frac{1}{\sqrt{f'(x)}}. \tag{19}$$

The discretization of variable x defined in $[-1,1]$ can be conveniently performed by taking advantage of the Gauss-type quadratures the abscissas and weights of which

depend further on the exact form of preassigned orthogonal polynomial [35]. In Ref. [37], the Legendre-Gauss-Lobatto quadrature is employed under which the integration of a polynomial with the order less than $2N-1$ is expressed by

$$\int_{-1}^{1} u(x)dx = \sum_{j=0}^{N} u(x_j)\omega_j, \tag{20}$$

where the abscissas read

$$x_0 = -1, \quad x_{j(j=1,\ldots,N-1)} = \text{zeros of } P'_N, \quad x_N = 1, \tag{21}$$

combined with the weights

$$\omega_j = \frac{2}{N(N+1)}\frac{1}{[P_N(x_j)]^2}. \tag{22}$$

$P_N(x)$ and $P'_N(x)$ denote the Nth-order Legendre polynomial and its first-order derivative, respectively.

The pseudospectral approximation implemented in the relativistic Dirac equation is similar to the one in the nonrelativistic Schrödinger equation. The two-component unknown function $\phi(x)$ is approximated by two Nth-order polynomials expressed in terms of superposition of cardinal functions

$$\begin{aligned}\begin{pmatrix} p(x) \\ q(x) \end{pmatrix} &= \phi(x) \approx \phi_N(x) = \sum_{j=0}^{N} g_j(x)\phi(x_j) \\ &= \sum_{j=0}^{N}\left[\begin{pmatrix} g_j(x) \\ 0 \end{pmatrix} p(x_j) + \begin{pmatrix} 0 \\ g_j(x) \end{pmatrix} q(x_j)\right], \end{aligned} \tag{23}$$

where x_j are the abscissas defined in Eq. (21) and $g_j(x)$ are shifted deltalike cardinal functions which fulfill the condition $g_j(x_i) = \delta_{ij}$. The cardinal functions can be conveniently constructed from the Lagrange polynomials defined at the collocation points:

$$g_j(x) = \frac{1}{N(N+1)}\frac{(1-x^2)}{(x_j-x)}\frac{P'_N(x)}{P_N(x_j)}. \tag{24}$$

The substitution of Eq. (23) into Eq. (18) leads to the discretized equation formally written as

$$\sum_{j=0}^{N}[h_D(x)g_j(x)]\phi(x_j) = E\sum_{j=0}^{N} g_j(x)\phi(x_j). \tag{25}$$

As shown in Ref. [35] and our previous work [47], the first-order derivative of a function $u(x)$ at collocation points can be approximated by

$$\frac{d}{dx}u(x)|_{x=x_i} = \sum_{j=0}^{N}(d_1)_{ij}\frac{P_N(x_i)}{P_N(x_j)}u(x_j), \tag{26}$$

where

$$(d_1)_{ij} = \begin{cases} -\frac{1}{x_i-x_j} & (i \neq j) \\ 0 & (i = j \in [1, N-1]) \\ -\frac{(N+1)N}{4} & (i = j = 0) \\ \frac{(N+1)N}{4} & (i = j = N) \end{cases}. \tag{27}$$

Therefore, the corresponding eigenvalue problem associated with Eq. (25) is given by

$$[\mathbf{h_D}][\boldsymbol{\phi}] = [\mathbf{E}][\boldsymbol{\phi}], \tag{28}$$

where the Hamiltonian matrix element reads

$$\begin{aligned}(h_D)_{ij} = &\begin{pmatrix} V[f(x_i)] + c^2 & c\frac{\kappa}{f(x_i)} \\ c\frac{\kappa}{f(x_i)} & V[f(x_i)] - c^2 \end{pmatrix}\delta_{ij} \\ &+ \begin{pmatrix} 0 & -c \\ c & 0 \end{pmatrix}\frac{1}{\sqrt{f'(x_i)}}(d_1)_{ij}\frac{1}{\sqrt{f'(x_j)}}\frac{P_N(x_i)}{P_N(x_j)}, \end{aligned} \tag{29}$$

and $[\boldsymbol{\phi}]$ is a column vector in $2(N+1)$ dimension.

As in the nonrelativistic situation, one can further simplify the eigenvalue problem by utilizing the symmetric transformations

$$A_j = \frac{\phi(x_j)}{P_N(x_j)} = \frac{\sqrt{f'(x_j)}\psi[f(x_j)]}{P_N(x_j)}, \tag{30}$$

and

$$\begin{aligned}(H_D)_{ij} =& \; h_{Dij}\frac{P_N(x_j)}{P_N(x_i)} \\ =& \begin{pmatrix} V[f(x_i)] + c^2 & c\frac{\kappa}{f(x_i)} \\ c\frac{\kappa}{f(x_i)} & V[f(x_i)] - c^2 \end{pmatrix}\delta_{ij} \\ &+ \begin{pmatrix} 0 & -c \\ c & 0 \end{pmatrix}\frac{1}{\sqrt{f'(x_i)}}(d_1)_{ij}\frac{1}{\sqrt{f'(x_j)}}. \end{aligned} \tag{31}$$

The resulting eigenvalue problem is a standard and symmetric one which formally reads

$$[\mathbf{H_D}][\mathbf{A}] = [\mathbf{E}][\mathbf{A}]. \tag{32}$$

It is interesting to note that although the matrix (d_1) is nonsymmetric, the transformed Hamiltonian matrix $[\mathbf{H_D}]$ is symmetric and, therefore, both the eigenvalues and eigenvectors are real-defined. Recalling the asymptotic behavior of radial wave functions at $r = 0$ [Eq. (11)] and the natural boundary condition for $r \to \infty$ [Eq. (12)], it is clear that $A_0 = A_N = 0$ and the dimension of the standard symmetric eigenvalue problem is $2(N-1)$.

C. Algebraic mapping function

As mentioned above, the mapping function utilized in Eq. (14) is the same as the one used in the Schrödinger equation. The significant advantage of such a formalism rests on the simplification of the second-order differential operator by vanishing the remaining term U_m [39] in the kinetic-energy operator:

$$U_m(x) = \frac{3f''^2 - 2f'''f'}{8f'^4} \overset{\text{[Eq. (14)]}}{=} 0. \tag{33}$$

However, in the Dirac equation, there is not a second-order differential term and the utilization of other mapping functions would not introduce any more complexities. In this paper, we would like to employ the mapping function in a

general form:

$$r = f(x) = L\frac{(1+x)^k}{1-x}, \tag{34}$$

where the power k provides further control of the distribution of mesh points in the semi-infinite domain. A larger value of k produces denser grids in the close range, but sparser grids in the far range, which means that more grid points are distributed in regions close to both zero and ∞ [60]. The generalized mapping function provides us additional flexibility in applying the GPS method, e.g., to calculate the high-lying excited Rydberg states as well as to investigate the finite-size effect of different nuclear models on the electronic states.

D. Kinetically balanced condition

A variety of techniques that were developed to tackle the problem of spurious states have been summarized in the introduction. The introduction of specific boundary conditions or additional Wilson terms does not remove the spurious states but lifts them up onto the top of the spectrum. The construction of radial wave functions on alternating grids as in the finite-difference method seems to be more cumbersome when it is applied to the GPS method. On the other hand, inspired by the fact that the spectral approximation shown in Eq. (23) can be equivalently treated as a special basis-set expansion method in terms of cardinal functions $g_j(x)$ and coefficients $\phi(x_j)$, it would be a rather natural choice to incorporate the kinetically balanced condition into the GPS method to remove the spurious states.

1. Mono kinetic balance

It is convenient to rewrite the two-component basis functions in the form

$$u_i(r) = \begin{cases} \begin{pmatrix}\pi_i(r)\\ 0\end{pmatrix} & (1 \leqslant i \leqslant n) \\ \begin{pmatrix}0\\ \pi_{i-n}(r)\end{pmatrix} & (n+1 \leqslant i \leqslant 2n). \end{cases} \tag{35}$$

The extensively used "mono" kinetically balanced (MKB) condition [24] only imposes constraints on those basis functions used to construct the lower component of the radial wave function:

$$u'_i(r) = \begin{cases} \begin{pmatrix}\pi_i(r)\\ 0\end{pmatrix} & (1 \leqslant i \leqslant n) \\ \begin{pmatrix}0\\ D^+\pi_{i-n}(r)\end{pmatrix} & (n+1 \leqslant i \leqslant 2n), \end{cases} \tag{36}$$

where the operator D^+ reads

$$D^+ = \frac{1}{2c}\left(\frac{d}{dr} + \frac{\kappa}{r}\right). \tag{37}$$

The relationship between the upper and lower components of the basis function ensures that the Dirac equation would reduce to the ordinary Schrödinger equation in the nonrelativistic limit (under the condition $|E - c^2| \ll 2c^2$). The corresponding solutions of the secular equations based on u_i and u'_i, respectively, with the same eigenenergy are eigenvectors c_i and c'_i. Due to the fact that $\psi = \sum_i c_i u_i = \sum_i c'_i u'_i$, the new kinetically balanced basis set can be formally written as

$$[\mathbf{u}'] = [\mathbf{u}]\begin{pmatrix}\mathbf{I} & 0\\ 0 & \mathbf{D}^+\end{pmatrix}, \tag{38}$$

where both $[\mathbf{u}]$ and $[\mathbf{u}']$ are row vectors, $\mathbf{I}$ is the unit matrix, and $\mathbf{D}^+$ is a diagonal matrix with its elements being D^+. The operator matrix including $\mathbf{D}^+$ acts on $[\mathbf{u}]$ from right to left so that Eq. (36) can be successfully reproduced. The expansion coefficients simply have the relation

$$[\mathbf{c}] = \begin{pmatrix}\mathbf{I} & 0\\ 0 & \mathbf{D}^+\end{pmatrix}[\mathbf{c}']. \tag{39}$$

The core step in introducing the MKB condition into the GPS method relies on the fact that the eigenvectors to be calculated in the pseudospectral approximation [in Eq. (23)] are the radial wave functions themselves (at collocation points). In this sense, it can be generally considered that the wave functions in the GPS method play the same role as the eigenvectors in the basis-set expansion method. Following the same way as shown in Eq. (39), the MKB condition can be directly imposed on the radial wave function, which yields

$$\begin{pmatrix}P(r)\\ Q(r)\end{pmatrix} = \begin{pmatrix}1 & 0\\ 0 & D^+\end{pmatrix}\begin{pmatrix}P'(r)\\ Q'(r)\end{pmatrix}, \tag{40}$$

keeping in mind that the operator matrix employed here is two-dimensional. Substitution of the above equation into Eq. (6) leads to the MKB radial Dirac equation:

$$\begin{pmatrix}V(r)+c^2 & -c\left(\frac{d}{dr} - \frac{\kappa}{r}\right)\\ c\left(\frac{d}{dr} + \frac{\kappa}{r}\right) & V(r)-c^2\end{pmatrix}\begin{pmatrix}1 & 0\\ 0 & D^+\end{pmatrix}\begin{pmatrix}P'_{n\kappa}(r)\\ Q'_{n\kappa}(r)\end{pmatrix} = E\begin{pmatrix}1 & 0\\ 0 & D^+\end{pmatrix}\begin{pmatrix}P'_{n\kappa}(r)\\ Q'_{n\kappa}(r)\end{pmatrix}. \tag{41}$$

By performing similar mapping transformations for the radial variables and wave function as we did in Sec. II B, the new coupled radial equation with respect to x now reads

$$h'_D(x)\phi'(x) = EO'(x)\phi'(x), \tag{42}$$

where

$$\begin{aligned} h'_D(x) = &\begin{pmatrix}V+c^2 & \frac{\kappa(\kappa+1)}{2f^2(x)}\\ c\frac{\kappa}{f(x)} & \frac{V-c^2}{2c}\frac{\kappa}{f(x)}\end{pmatrix} \\ &+ \begin{pmatrix}0 & 0\\ c & \frac{V-c^2}{2c}\end{pmatrix}\frac{1}{\sqrt{f'(x)}}\frac{d}{dx}\frac{1}{\sqrt{f'(x)}} \\ &+ \begin{pmatrix}0 & -\frac{1}{2}\\ 0 & 0\end{pmatrix}\frac{1}{f'(x)}\frac{d^2}{dx^2}\frac{1}{f'(x)}, \end{aligned} \tag{43}$$

and

$$O'(x) = \begin{pmatrix}1 & 0\\ 0 & \frac{1}{2c}\frac{\kappa}{f(x)}\end{pmatrix} + \begin{pmatrix}0 & 0\\ 0 & \frac{1}{2c}\end{pmatrix}\frac{1}{\sqrt{f'(x)}}\frac{d}{dx}\frac{1}{\sqrt{f'(x)}}. \tag{44}$$

The algebraic, first-order, and second-order differential terms in the above derivations are separated from each other for programming convenience. The implementation of the subsequent pseudospectral approximation and variable discretization is the same as before, except that there exists the second-order derivative of a function at the collocation points. This is not new but the same as the one developed in the nonrelativistic GPS method [35,47]:

$$\frac{d^2}{dx^2}u(x)|_{x=x_i} = \sum_{j=0}^{N}(d_2)_{ij}\frac{P_N(x_i)}{P_N(x_j)}u(x_j), \tag{45}$$

where

$$(d_2)_{ij}=\begin{cases}-\frac{2}{(x_i-x_j)^2} & (i\neq j, i\in[1,N-1],\ j\in[0,N])\\ -\frac{N(N+1)}{3(1-x_i^2)} & (i=j\in[1,N-1])\\ \frac{N(N+1)(N^2+N-2)}{24} & (i=j=(0\text{ or }N))\\ \frac{N(N+1)(1+x_j)-4}{2(1+x_j)^2} & (i=0,\ j\in[1,N])\\ \frac{N(N+1)(1-x_j)-4}{2(1-x_j)^2} & (i=N,\ j\in[0,N-1]).\end{cases} \tag{46}$$

Due to the appearance of the second-order derivative with respect to r in the radial equation Eq. (41), it should be kept in mind that, when the mapping function of Eq. (34) with $k\neq 1$ is utilized, one must supplement the diagonal term $-2U_m(x)$ [39] to the second-order derivative with respect to x on the right-hand side of Eq. (43). The derivation of $U_m(x)$ shown in Eq. (33) with respect to different mapping functions is quite straightforward and will not be presented here. In what follows, this method will be referred to as the mono kinetically balanced generalized pseudospectral method (MKB-GPS).

The associated eigenvalue problem is expressed as

$$[\mathbf{h}_\mathbf{D}'][\boldsymbol{\phi}']=[\mathbf{E}][\mathbf{O}'][\boldsymbol{\phi}'], \tag{47}$$

which is *formally* the same as the generalized eigenvalue problem in the basis-set expansion method with nonorthogonal basis functions. One must keep in mind that the matrix $[\mathbf{O}']$ does not signify the overlap matrix and this fact is the intrinsic difference between the basis-set expansion and the kinetically balanced GPS methods. Once the eigenenergy is obtained, a back transformation on the eigenvector formulated in Eq. (40) is necessary to get the relativistic radial wave function defined directly on the grid points.

2. Dual kinetic balance

The "dual" kinetically balanced (DKB) condition initiated by Shabaev *et al.* [13] imposes the kinetic matching constraints onto both the upper and lower components of the radial wave function. The new basis set corresponding to Eq. (36) is given by

$$u_i''(r)=\begin{cases}\begin{pmatrix}\pi_i(r)\\ D^+\pi_i(r)\end{pmatrix} & (1\leqslant i\leqslant n)\\ \begin{pmatrix}D^-\pi_{i-n}(r)\\ \pi_{i-n}(r)\end{pmatrix} & (n+1\leqslant i\leqslant 2n),\end{cases} \tag{48}$$

where D^+ is available in Eq. (37) and D^- reads

$$D^-=\frac{1}{2c}\left(\frac{d}{dr}-\frac{\kappa}{r}\right). \tag{49}$$

The profits of utilizing the dual kinetically balance condition rest on several aspects: (a) the basis set is symmetric with respect to the replacement of $\kappa\to-\kappa$ and the interchange of upper and lower components, (b) the basis functions in $1\leqslant i\leqslant n$ and $n+1\leqslant i\leqslant 2n$ provide correct relations between the upper and lower components for positive and negative energies, respectively, and (c) the spurious states in both the attractive and repulsive potentials can be removed.

Following a similar procedure as in the MKB-GPS method, the dual condition implies a transformation on the radial wave function:

$$\begin{pmatrix}P(r)\\ Q(r)\end{pmatrix}=\begin{pmatrix}1 & D^-\\ D^+ & 1\end{pmatrix}\begin{pmatrix}P''(r)\\ Q''(r)\end{pmatrix}. \tag{50}$$

The resulting radial Dirac equation in variable r yields

$$\begin{pmatrix}V(r)+c^2 & -c\left(\frac{d}{dr}-\frac{\kappa}{r}\right)\\ c\left(\frac{d}{dr}+\frac{\kappa}{r}\right) & V(r)-c^2\end{pmatrix}\begin{pmatrix}1 & D^-\\ D^+ & 1\end{pmatrix}\begin{pmatrix}P''_{n\kappa}(r)\\ Q''_{n\kappa}(r)\end{pmatrix}=E\begin{pmatrix}1 & D^-\\ D^+ & 1\end{pmatrix}\begin{pmatrix}P''_{n\kappa}(r)\\ Q''_{n\kappa}(r)\end{pmatrix}, \tag{51}$$

and in variable x it reads

$$h_D''(x)\phi''(x)=EO''(x)\phi''(x), \tag{52}$$

where

$$\begin{aligned}h_D''(x)=&\begin{pmatrix}V+c^2+\frac{\kappa(\kappa+1)}{2f^2(x)} & -\frac{V-c^2}{2c}\frac{\kappa}{f(x)}\\ \frac{V+c^2}{2c}\frac{\kappa}{f(x)} & V-c^2-\frac{\kappa(\kappa-1)}{2f^2(x)}\end{pmatrix}\\ &+\begin{pmatrix}0 & \frac{V-c^2}{2c}\\ \frac{V+c^2}{2c} & 0\end{pmatrix}\frac{1}{\sqrt{f'(x)}}\frac{d}{dx}\frac{1}{\sqrt{f'(x)}}\\ &+\begin{pmatrix}-\frac{1}{2} & 0\\ 0 & \frac{1}{2}\end{pmatrix}\frac{1}{f'(x)}\frac{d^2}{dx^2}\frac{1}{f'(x)},\end{aligned} \tag{53}$$

and

$$\begin{aligned}O''(x)=&\begin{pmatrix}1 & -\frac{1}{2c}\frac{\kappa}{f(x)}\\ \frac{1}{2c}\frac{\kappa}{f(x)} & 1\end{pmatrix}\\ &+\begin{pmatrix}0 & \frac{1}{2c}\\ \frac{1}{2c} & 0\end{pmatrix}\frac{1}{\sqrt{f'(x)}}\frac{d}{dx}\frac{1}{\sqrt{f'(x)}}.\end{aligned} \tag{54}$$

As before, a diagonal term $-2U_m(x)$ must be supplemented to the second-order derivative with respect to x on the right-hand side of Eq. (53) if a mapping function with $k\neq 1$ is employed. The associated eigenvalue problem is similar to Eq. (47):

$$[\mathbf{h}_\mathbf{D}''][\boldsymbol{\phi}'']=[\mathbf{E}][\mathbf{O}''][\boldsymbol{\phi}''], \tag{55}$$

which is a generalized nonsymmetric eigenvalue problem. Even though both $[\mathbf{h}_\mathbf{D}'']$ and $[\mathbf{O}'']$ are nonsymmetric, we do not encounter the occurrence of complex eigenvalues and eigenvectors in our numerical calculations. A rigorous proof of such a property warrants further studies. The back transformation of Eq. (50) should be performed to get the final radial wave function. In the following discussion, this method will be denoted as the dual kinetically balanced generalized pseudospectral method (DKB-GPS).

E. Atomically balanced condition

The operators D^+ and D^- are obtained elsewhere to remove the spurious solutions in solving the Dirac equation; however, we show in Appendix A that they can be alternatively derived from the operators which explicitly include the interaction potential, i.e.,

$$D_V^+=\frac{1}{2c-\frac{V(r)}{c}}\left(\frac{d}{dr}+\frac{\kappa}{r}\right), \tag{56}$$

and

$$D_V^- = \frac{1}{2c + \frac{V(r)}{c}}\left(\frac{d}{dr} - \frac{\kappa}{r}\right), \tag{57}$$

under the condition $|V(r)| \ll 2c^2$. The constraints employing D_V^+ and D_V^- are generally named as the atomically balanced conditions. The replacement of D^+ and D^- by D_V^+ and D_V^-, respectively, in the above derivations of MKB-GPS and DKB-GPS leads to the mono atomically balanced GPS (MAB-GPS) and dual atomically balanced GPS (DAB-GPS) methods.

The atomically balanced condition has been employed by Visscher *et al.* [61] to build the contracted basis sets based on Gaussian-type orbitals. It has been shown that the application of the atomically balanced condition is a better choice for heavily contracted basis functions, because the kinetically balanced condition would lead to serious numerical problems and sometimes incorrect results. Such a phenomenon is not surprising because the potential operators in Eqs. (56) and (57) are increasingly important for systems with high nuclear charges. This condition has been adopted by Kozlov and Tupitsyn [62] to construct the mixed basis sets based on B-splines in their investigations on heavy atoms. The atomically balanced B-spline basis functions have also been developed by Fillion-Gourdeau *et al.* [63] in the Galerkin approximation of the time-independent and time-dependent Dirac equations for one-electron diatomic molecules, and it was concluded by these authors that the atomic balance is more relevant than the kinetic one to eliminate the variational collapse in heavy ions.

The drawback of the atomically balanced condition, in the basis-set expansion methods, is largely attributed to the difficulties in numerical or analytical computation of the Hamiltonian and overlap matrix elements due to the explicit appearance of potential operators in basis functions. Furthermore, the utilization of atomic balance in the time-dependent investigations of laser-atom interactions would also lead to additional singularities [63]. These are probably the reasons for the less popular atomic condition than the kinetic one. However, as we show in Appendix B, the incorporation of either mono or dual atomically balanced conditions in the framework of GPS method is quite straightforward provided that some efforts need to be paid in the construction of the transformed Dirac equation.

III. RESULTS AND DISCUSSION

A. Bound states with $\kappa < 0$

Solutions of the Dirac equation with negative quantum number κ by numerical methods do not have spurious states, so they are suitable to use in testing the accuracy of the relativistic GPS method. The relative errors of calculated energies for H-like ions with point-charge nuclei are defined by

$$\delta_E = \left|\frac{E_{\rm GPS} - E_{\rm exact}}{E_{\rm exact}}\right|, \tag{58}$$

where $E_{\rm exact}$ is given in Eq. (9). In the present paper, all numerical calculations are performed in quadruple precision (≈34 significant digits after the decimal point). Results for the series of $s_{1/2}$ bound states of the H atom are displayed in Figs. 1(a), 1(b) and 1(c) with respect to the parameters N, L, and k,

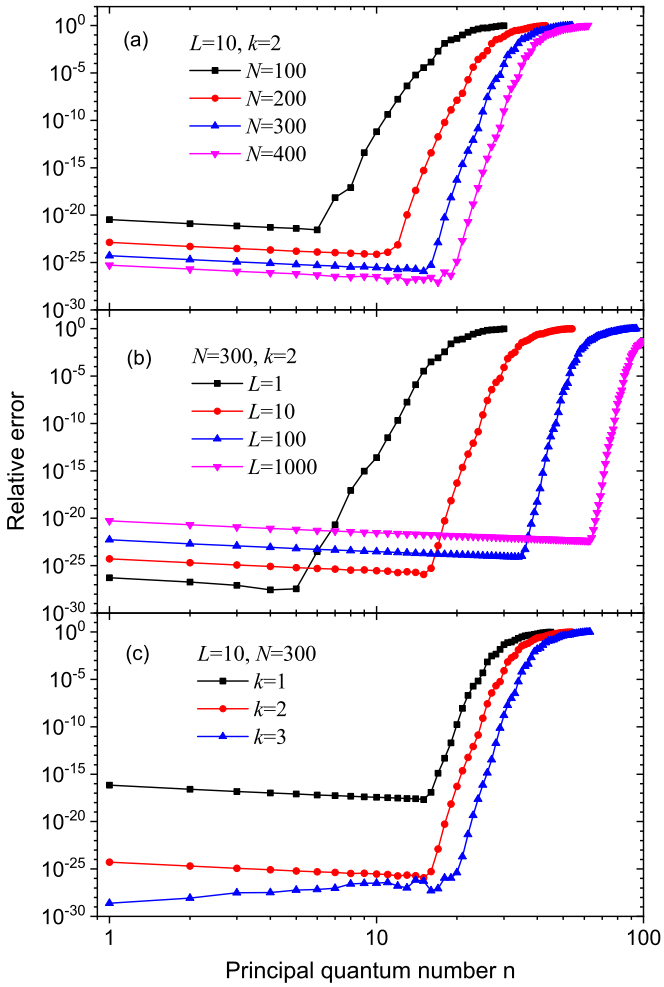

FIG. 1. Energy relative errors of the $s_{1/2}$ states of the H atom calculated by using different mapping functions. (a) Fixed L and k with different N, (b) fixed N and k with different L, and (c) fixed L and N with different k.

respectively. For a specific mapping function, i.e., by fixing L and k as shown in Fig. 1(a), the increasing of the number of grid points would generally increase the accuracy for all bound states and, furthermore, extend the applicability of GPS method to higher-lying excited states. In Fig. 1(b), N and k are fixed and the mapping parameter L is enlarged gradually. It is known from Eq. (34) that L equally separates the number of grid points into subdomains $[0, L]$ and $[L, \infty]$. Therefore, the increasing of L would lead to sparser distribution of grids in the entire space, i.e., less points in smaller regions and more points in extensively large regions. It can be anticipated that, at relatively large L, the accuracy of lower-lying states would decrease, while those for higher-lying ones increase. The effect of mapping parameter k which further adjusts the nonlinear distribution of grid points is shown in Fig. 2, where a total number of 19 grid points ($N = 20$) with respect to $k = 1$, 2, and 3 are demonstrated schematically. By increasing k, the grid points are expanded into both close and far regions which should manifest a better description of the asymptotic behaviors of the radial wave functions at both $r \to 0$ and ∞. However, the density of grid points around L would inevitably

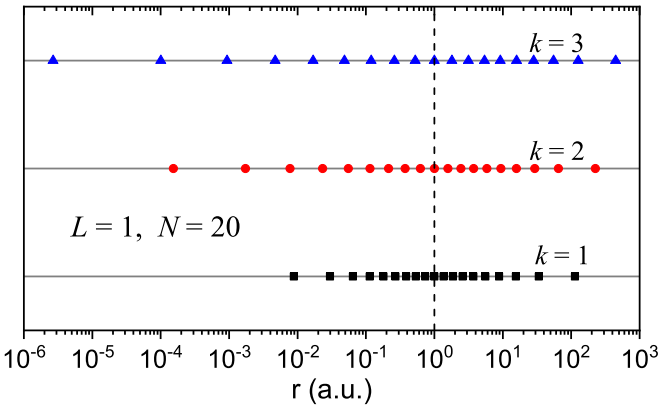

FIG. 2. Demonstration of the distribution of grid points by using different mapping functions with parameters $N = 20$, $L = 1$, and $k = 1$–3. The vertical line represents the location ($r = L$) that equally separates the number of grid points.

be reduced. From Fig. 1(c) it is clear that for a moderate value of N, the use of $k = 2$ systematically improves the accuracy of calculations more than those with $k = 1$. The use of $k = 3$ may improve the calculation further, but some instabilities show up for high-lying excited states. Such a phenomenon will be revisited in the following discussion.

Keeping in mind that the predictions shown in Fig. 1 for a specific group of parameters (N, L, and k) are obtained by a single-time solution of the eigenvalue problem, the accuracy and efficiency of the relativistic GPS method can be fairly guaranteed, i.e., with a moderate number of grid points one can simultaneously access system bound states from low- to high-lying excitation with similar high accuracy. In Fig. 3, the upper and lower components of radial wave functions for $s_{1/2}$ states with principal quantum numbers being 1, 5, 10, 20, and 30 are illustrated and compared with the analytical solutions [58]. The accuracy of energies for these states generally lies in 10^{-23}–10^{-25} compared to the exact values. One can see that the numerical calculations of wave functions show a perfect agreement with the analytical ones in the entire range of radius. For highly excited Rydberg states, the upper and lower components of the radial wave function show drastic oscillations with the former and latter ones having large amplitudes in the far and close regions, respectively. An effective and equally important treatment of the asymptotic behaviors in both far and close regions plays a vital role in such demanding calculations.

The relativistic GPS method also shows its capability in predicting bound states with high angular momentum. In Fig. 4, the energy relative errors of bound states with negative Dirac quantum numbers ($-6 \leqslant \kappa \leqslant -1$) are displayed together for a comparative purpose. It is interestingly found that the non-s-wave states follow a different trend from the s-wave states and show better accuracy. The relatively large errors in $s_{1/2}$ states compared to those with higher angular momenta probably come from two aspects: (1) the slower decreasing speed of radial wave functions when they approach the origin [as one can see from Eq. (11), the power term γ is less than 1 in $s_{1/2}$ states, while it becomes increasingly greater than 1 in non-s-wave states] and (2) the singularity of the Dirac wave function at $r = 0$, because of which the pseudospectral polynomial approximation of the first-order derivative shown in Eq. (26) may not be very accurate. For states with $\kappa \leqslant -2$, instabilities of the relative errors are observed in high-lying excited states which are similar to those displayed in Fig. 1(c) with $k = 3$. It is conjectured that such a phenomenon is primarily caused by an inappropriate description of the exponential decay of radial wave functions as $r \to \infty$. In the inset of Fig. 4, we illustrate the numerically calculated upper and lower components of the radial wave function for the $2p_{3/2}$ state and their exact asymptotic laws

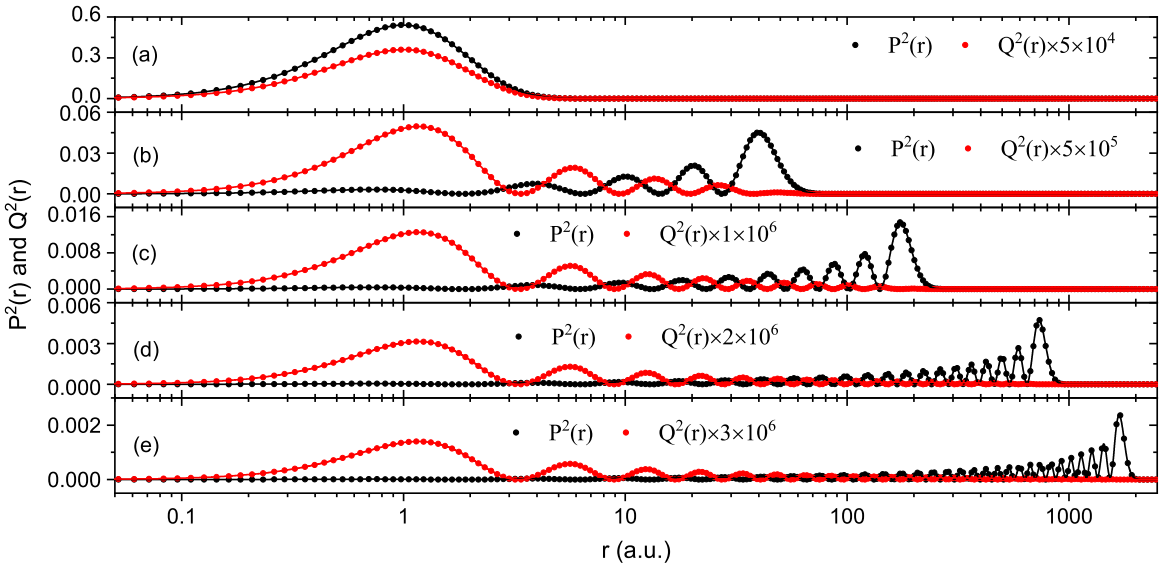

FIG. 3. Radial wave functions for some $s_{1/2}$ states of the H atom calculated with the mapping parameters $N = 300$, $L = 100$, and $k = 2$. Lower components of radial wave functions are scaled for a clear view. Dots represent the present numerical calculations and solid lines refer to the analytical solutions. (a) $1s_{1/2}$ state with energy relative error $\delta_E = 5.39 \times 10^{-23}$, (b) $5s_{1/2}$ state with $\delta_E = 6.46 \times 10^{-24}$, (c) $10s_{1/2}$ state with $\delta_E = 2.95 \times 10^{-24}$, (d) $20s_{1/2}$ state with $\delta_E = 1.40 \times 10^{-24}$, and (e) $30s_{1/2}$ state with $\delta_E = 8.96 \times 10^{-25}$.

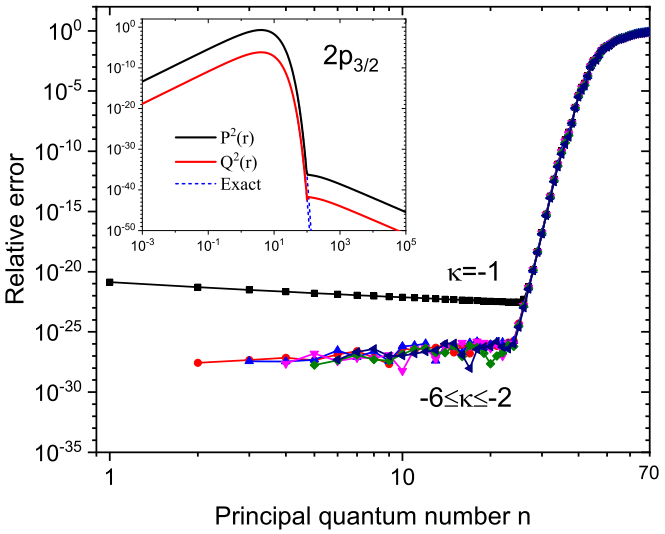

FIG. 4. Energy relative errors of the negative κ states of the H atom calculated with mapping parameters $N = 200$, $L = 100$, and $k = 2$. The inset displays the upper and lower components of the radial wave function for the $2p_{3/2}$ state the exact asymptotic forms of which are exponential.

shown in Eq. (12). The overestimate of radial wave functions at large r corresponds to the fact that, for the GPS method formulated in DVR, the N-th-order Gauss quadrature is only accurate for polynomials with orders up to $2N - 1$ [35,36]. The consequence of such criteria is that one cannot reproduce the exponential asymptotic behavior of the radial wave function by using a finite number of points. From the computational aspect, one can always increase N to improve the agreement at larger r and abandon the remaining part that behaves incorrectly. The induced errors in practical calculations of bound-state properties are expected to be small due to the small magnitude of the wave function in this far region. One may further notice that the exponential laws shown in Eq. (12) are different for states with different principal quantum number n. Consequently, the numerical errors imported by the asymptotic region may contribute diversely for different states which results in instabilities in the relative errors shown in Fig. 4. This defect, however, does not appear visibly in the $s_{1/2}$ states (specified to the parameters used in Fig. 4). This is probably due to their smaller contributions compared to the slow convergence and singularity of the radial wave function near $r = 0$. With more elaborate representation of the wave functions at small r, as we did in Fig. 1(c) by using $N = 300$ and the mapping parameter $k = 3$, the instabilities start to dominate. The criticism mentioned above should not affect the robustness and efficiency of the relativistic GPS method. By using a moderate number of grid points (e.g., $N = 200$) and solving the eigenvalue problem one time per angular momentum, one can directly access a large series (e.g., $n \leqslant 28$) of s-wave and non-s-wave states with their energy accuracy lying in 10^{-21}–10^{-23} and 10^{-26}–10^{-28}, respectively. Such accuracy goes far beyond the requirement in most atomic property calculations.

B. Bound states with $\kappa > 0$

The calculation of bound states with positive Dirac quantum number κ is much more involved due to the appearance of spurious states. In the original GPS calculations of the Dirac equation with exact Coulomb potential, there always exists a single spurious state located at the bottom of the spectrum for the Hamiltonian with positive κ. It has surprisingly the same energy as the lowest physical state with $-\kappa$. The origin of the spurious state has been extensively discussed by many authors [11,12,21,26,61] and it can be summarized that the spurious state emerges when the Dirac equation is approximately solved in a model space of finite dimension. The GPS method with a finite number of grid points belongs to such a situation. Here we further provide a simple way to understand the behavior of the spurious state specialized to the pure Coulomb potential. It is known that for bound states with $n = |\kappa|$ the lower component of the radial wave function is connected with the larger one by a constant [58]. We can simply write

$$P(r) = CQ(r). \tag{59}$$

The substitution of the above equation into Eq. (6) leads to the coupled radial equations

$$\begin{aligned}(c^2 - E + V)CQ(r) &= c\left(\frac{d}{dr} - \frac{\kappa}{r}\right)Q(r),\\ (c^2 + E - V)Q(r) &= c\left(\frac{d}{dr} + \frac{\kappa}{r}\right)CQ(r).\end{aligned} \tag{60}$$

Considering the exact Coulomb potential $V(r) = -1/r$, multiplying C onto the upper equation, and subtracting the lower equation by the upper one, we finally get an equality one side of which is a function of r while the other side is a constant:

$$(c^2 + E) - C^2(c^2 - E) = -\frac{1}{r}(C^2 - 2C\kappa c + 1). \tag{61}$$

It is a rather natural choice that both sides must be zero so that the equality validates at all r. The consequences are, respectively,

$$C^2 = \frac{c^2 + E}{c^2 - E}, \tag{62}$$

and

$$C^2 - 2C\kappa c + 1 = 0. \tag{63}$$

The substitution of Eq. (62) into Eq. (63) simply yields the expression for the constant C as

$$C = \frac{1}{\kappa}\frac{c}{c^2 - E} = -\frac{1}{\kappa}\frac{c}{\varepsilon}, \tag{64}$$

where the electronic energy ε (<0 for bound states) is defined in Eq. (2). With C available explicitly, it is easily derived from Eq. (60) that the asymptotic laws for the lower component of wave function $Q(r)$ read

$$\begin{aligned}Q_{n\kappa}(r) &\xrightarrow{r\to 0} r^{-\kappa(1+\frac{\varepsilon}{c^2})} \approx r^{-\kappa},\\ Q_{n\kappa}(r) &\xrightarrow{r\to\infty} e^{\frac{1}{\kappa}r}.\end{aligned} \tag{65}$$

Keeping in mind that the eigenenergy depends only on the magnitude of κ, Eq. (64) may lead to two independent solutions. For states with negative Dirac quantum numbers

($\kappa \leqslant -1$), the above expression corresponds to the fact that the lowest physical bound state of $n = -\kappa$ has a negative constant ($C < 0$) and behaves regularly at both the origin and infinity. In this case, Eq. (65) reproduces Eqs. (11) and (12) exactly. However, for states with positive Dirac quantum numbers ($\kappa \geqslant 1$), the solution with positive constant ($C > 0$) must be a spurious state because it becomes divergent near the origin and infinity. It is due to such a fact that the $n = \kappa$ states are abandoned in the analytical solutions. In other words, if there exists a spurious state in this system, its principal quantum number can be ambiguously identified as $n = \kappa$. In this situation, the spurious state has the same energy as the lowest physical bound state with their coefficients C having the same magnitude but opposite sign. It should be emphasized here that the above derivations are specified to the exact Coulomb potential. For general electron-nucleus potentials, e.g., the extended-charge nuclear potentials, the behavior of the spurious state may vary significantly.

In Figs. 5(a) and 5(b), respectively, the spurious and physical bound states with $n = |\kappa| = 1$ for the H atom are shown. One can further simplify the coefficient to be $|C| \approx 2c$ because of $\varepsilon \approx -1/2$. By multiplying a negative (positive) constant, the lower component of the radial wave function for the $1s_{1/2}$ physical ($1p_{1/2}$ spurious) state matches to the upper one perfectly. It is also noted that the physical state agrees perfectly with the analytical solution, while the spurious state diverges drastically near the origin [64]. It is reasonably conjectured that the spurious state may not be uniquely defined because it only needs to satisfy the energy equality, wave function matching, and asymptotic conditions. In Fig. 5, we further show the numerical calculations by employing a different group of parameters. It is clearly seen that the wave function of the spurious state is not unique, while the physical bound state is well converged.

The spurious states which exist in the relativistic GPS calculations can be successfully removed if additional constraints are enforced between the upper and lower components of the radial wave function. Based on the MKB- and DKB-GPS methods developed in Sec. II and the atomically balanced versions of the MAB- and DAB-GPS methods, we show in Figs. 6(a), 6(b) and 6(c), respectively, the energy relative errors of calculated bound states with Dirac quantum number $\kappa = 1, 2,$ and 3. The spurious state in the original GPS method has been omitted so that a meaningful comparison can be made. With usual input parameters ($N = 200$, $L = 100$, and $k = 1$), all four types of balanced GPS methods improve, or at least are not worse than, the original GPS calculations. In $p_{1/2}$ and $d_{3/2}$ states, the atomically balanced GPS methods are slightly better than the kinetically balanced ones and, moreover, they improve the prediction of energies by more than three orders of magnitude for $d_{3/2}$ states. In $f_{5/2}$ states, accuracy limits due to the inappropriate treatment of radial wave functions in the far asymptotic region are nearly achieved and all GPS calculations are in the same order of accuracy.

The comparison among different GPS methods may change from state to state, nevertheless they are not sensitive to the parameters N and L. However, this is not the case for the mapping function parameter k. In Fig. 7, similar calculations are performed with $k = 2$. As discussed earlier, the utilization

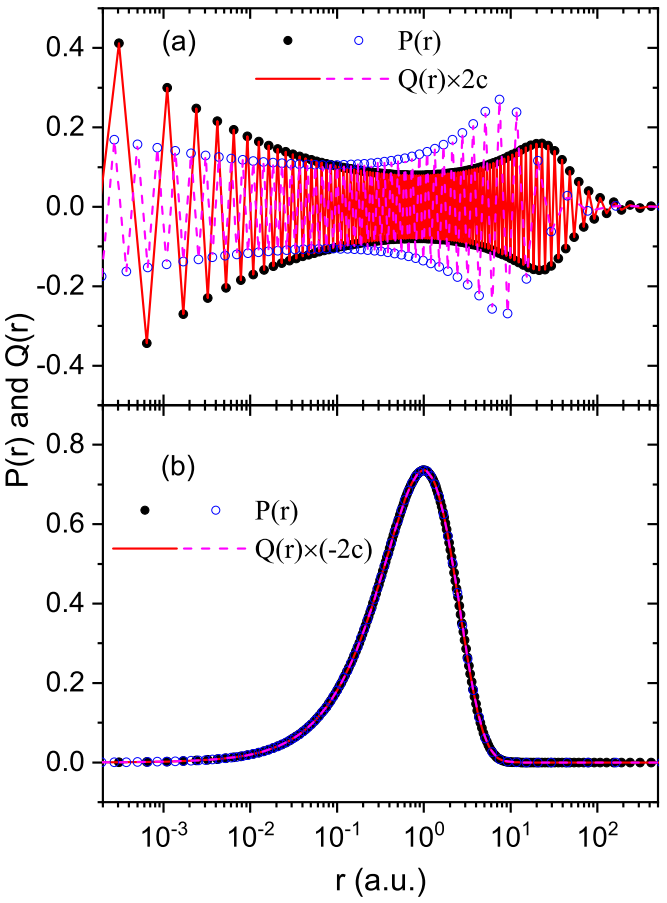

FIG. 5. Illustration of the $p_{1/2}$ ($\kappa = 1$) spurious state and the $1s_{1/2}$ ($\kappa = -1$) physical state of the H atom calculated with different mapping parameters: solid circle and line represent $N = 200$, $L = 1$, and $k = 1$; hollow circle and dash line refer to $N = 100$, $L = 0.1$, and $k = 2$. (a) Spurious $p_{1/2}$ state with calculated energy $E_{\rm spu}(p_{1/2}) = E(1s_{1/2}) = -0.500\,006\,656\,596\,552\,624$ a.u. (an accuracy of 3×10^{-18} compared to the exact value). (b) Physical $1s_{1/2}$ state. For both states, the lower components of radial wave functions are scaled by Eq. (59) to reproduce the upper components.

of larger k would expand the distribution of grid points into both close and far regions and, therefore, the calculation accuracy can be substantially improved even with a moderate value of grid points. Comparison between the original GPS calculations shown in Fig. 7 and those in Fig. 6 is similar to the $s_{1/2}$ states displayed in Fig. 1(c). It is generally found that the introduction of kinetically or atomically balanced conditions would reduce the accuracy of the GPS method by several orders of magnitude. The potential factor in atomically balanced conditions starts to take effect in all bound states, as we can see from the comparison between MKB-GPS and MAB-GPS calculations. Such phenomenon can be attributed to the fact that when more grid points are placed into the close vicinity of the nucleus, the singularity of the Coulomb potential becomes increasingly important and, therefore, the atomically balanced condition is more appropriate. The DKB-GPS results do not change much in the $p_{1/2}$ states compared to those with $k = 1$ shown in Fig. 6(a), but for $d_{3/2}$ and $f_{5/2}$ states they are generally in the same level of accuracy as that

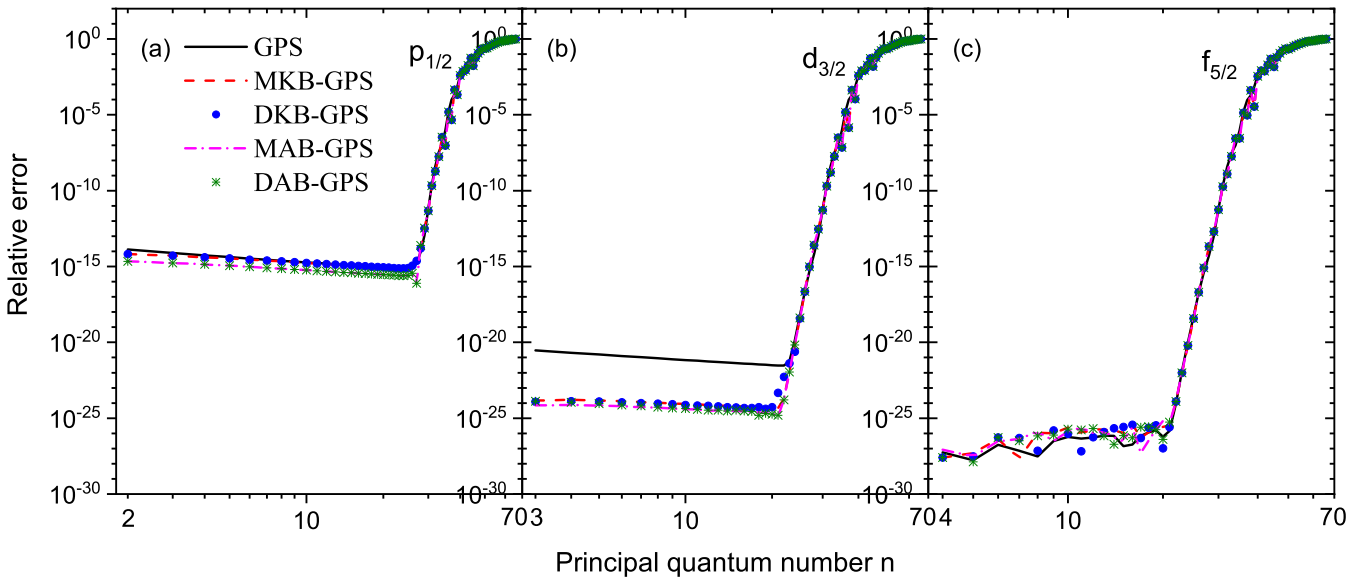

FIG. 6. Relative errors of the bound-state energies of the H atom with positive Dirac quantum number calculated by various GPS methods with mapping parameters $N = 200$, $L = 100$, and $k = 1$. (a) $p_{1/2}$ ($\kappa = 1$) states, (b) $d_{3/2}$ ($\kappa = 2$) states, and (c) $f_{5/2}$ ($\kappa = 3$) states.

in the calculations by MAB-GPS. One may ideally anticipate that the DAB-GPS method should be superior to DKB-GPS, as the MAB-GPS is doing better than MKB-GPS. However, it is found that the DAB-GPS calculations with such a mapping function are not stable enough. So they are not included here for comparison. Examining the matrix $O''(x)$ defined in Eq. (B9), one finds that its elements may have large negative values and, consequently, it is not always a positive definite matrix. Numerical solutions of such a generalized eigenvalue problem would produce complex eigenvalues with unexpected large imaginary parts. We suggest that the DAB-GPS method may not be suitable in calculations with the mapping functions $k \geqslant 2$.

Besides the system energies, it is also of interest to investigate the effect of kinetically and atomically balanced conditions on the radial wave functions. Figures 8(a) and 8(b) demonstrate, respectively, the large and small components of radial wave functions for $2p_{1/2}$ and $10p_{1/2}$ states with the same input parameters as those in Fig. 6(a). Also included here are the original GPS calculations with a larger number of grid points ($N = 300$). As one can see, the solely increasing N hardly improves the asymptotic behavior of radial wave functions. It is surprisingly found that, although the MKB-GPS and MAB-GPS methods only slightly improve the prediction of energy, they both amend the defect of radial wave functions in the far asymptotic region to a large extent. Such an

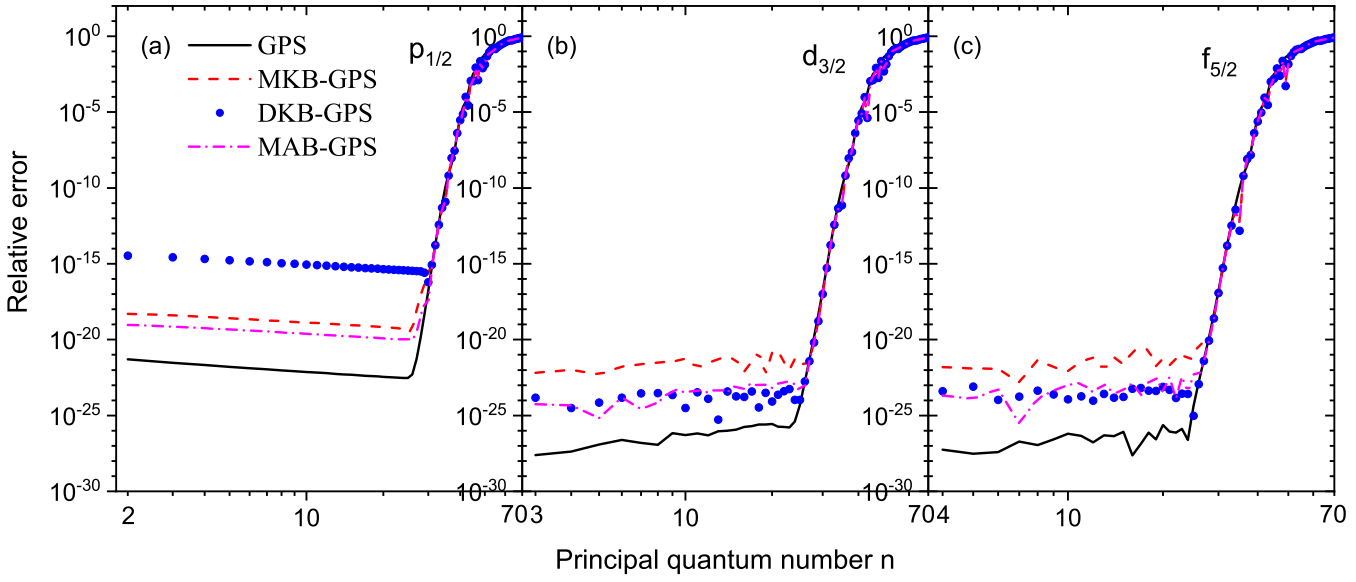

FIG. 7. Same as Fig. 6 except that $k = 2$ is used in the mapping function.

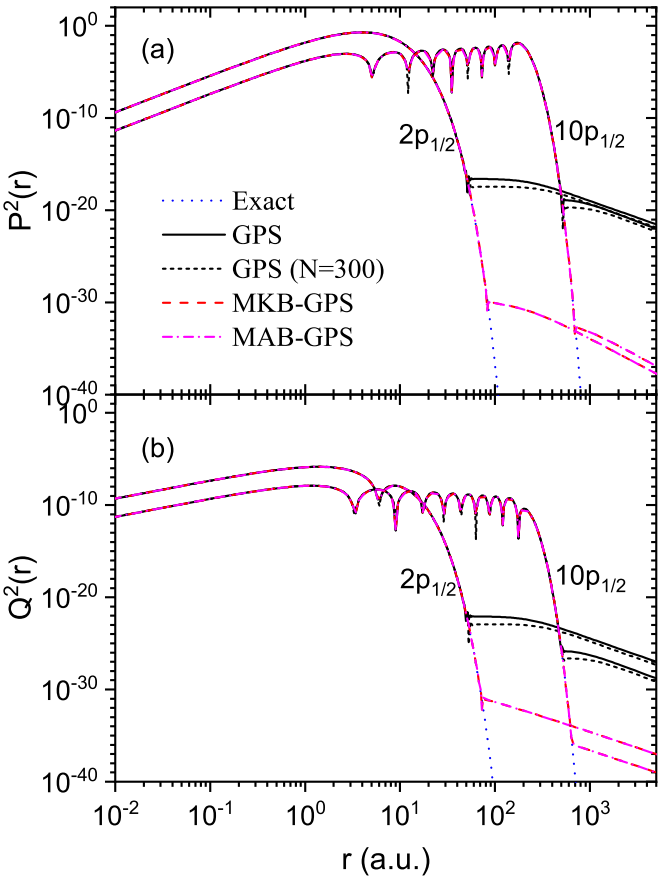

FIG. 8. Radial wave functions of the $2p_{1/2}$ and $10p_{1/2}$ states of the H atom calculated by various GPS methods with mapping parameters $N = 200$, $L = 100$, and $k = 1$. Blue dot lines represent the exact radial wave functions obtained analytically, and the black dash lines refer to the GPS calculations with more grid points $N = 300$. The MKB-GPS and MAB-GPS results are indistinguishable in the present figure scale. (a) Upper component and (b) lower component.

improvement of wave function at large r may have small contributions to the eigenenergy due to their small magnitudes. Nevertheless, a better description of the radial wave function in the asymptotic far region manifests the priority of kinetically and atomically balanced GPS methods in investigating the physical properties that are sensitive to the long-range behavior of wave functions. The comparison of wave functions with higher angular momenta are similar to those shown in Fig. 8 and they are omitted here.

From the comparison of system energies shown in Figs. 6 and 7 and the wave functions in Fig. 8, it is generally concluded that, when the most common mapping function of $k = 1$ is adopted, the four balanced GPS methods developed here would improve the prediction of system energies and wave functions compared to the original GPS method and, at the same time, eliminate the spurious states. For the mapping function with $k \geqslant 2$, the MAB-GPS method shows a slightly better performance than the others.

C. Highly charged ions with point-charge nuclear model

It is interesting to investigate the effect of kinetically and atomically balanced conditions in the calculation of highly charged ions where the singularity of the Coulomb potential near the origin is more pronounced. In Fig. 9, the energy relative errors of $p_{1/2}$ states for H-like ions with $Z = 1$, 10, and 50 are displayed in (a), (b), and (c), respectively. The point-charge nuclear model is used in all these systems. $N = 200$ and $k = 1$ are used throughout the calculations, and a smaller value of L for ions with larger Z is adopted to reflect the overall contraction of wave functions into the nuclear region. The DAB-GPS method is not included for comparison due to its instability for highly charged ions. Again, the spurious states in the original GPS calculations are omitted. One can see that the MKB-GPS estimations are almost in the same accuracy as those by DKB-GPS, and both of them are slightly better than the original GPS method.

With the point-charge nuclear model, the MAB-GPS method shows the best performance in the estimation of system energies for highly charged ions. Such a result is not surprising due to the fact that the kinetically balanced operator adopted in Eq. (37) can be alternatively considered as an approximation of the atomically balanced one defined in Eq. (56). In Fig. 10, we show the similar calculations on $p_{1/2}$ states as those in Fig. 9 but employing the mapping function of $k = 2$. It is interesting to note that with increasing Z the accuracy of the MKB-GPS method approaches gradually to the original GPS method for lower-lying states, but the situation deteriorates for intermediate states. The DKB-GPS calculations are the worst and the results do not change significantly compared to those with the mapping function of $k = 1$. The MAB-GPS method surpasses both the MKB-GPS and DKB-GPS ones and, eventually, it exceeds the original GPS method in heavy ions. The comparison between Figs. 9 and 10 further indicates that for highly charged ions the use of the mapping function of $k = 2$ is preferred because of its better description of the radial wave functions in the near nucleus region.

D. Highly charged ions with extended nuclear models

For highly charged ions where the finite-size effect of the nucleus cannot be neglected, more realistic extended nuclear models should be applied. Therefore, it would be of great interest to investigate the effects of kinetically and atomically balanced conditions in practical investigations. The first extended nuclear model is the homogeneously charged sphere, i.e., the charge of the nucleus is uniformly distributed in a sphere of radius R_0 which is further related to the root-mean-square radius of the nucleus:

$$R_0 = \sqrt{\frac{5}{3}\langle R^2 \rangle}. \tag{66}$$

The charge density distribution in the uniform-sphere model (USM) is then given by [65]

$$\rho^{\mathrm{USM}}(R) = \begin{cases} \frac{3Z}{4\pi R_0^3} & (R \leqslant R_0) \\ 0 & (R > R_0) \end{cases}. \tag{67}$$

After performing the integration over R in the entire space

$$V(r) = -\int d^3R \frac{\rho(R)}{|\boldsymbol{r} - \boldsymbol{R}|}, \tag{68}$$

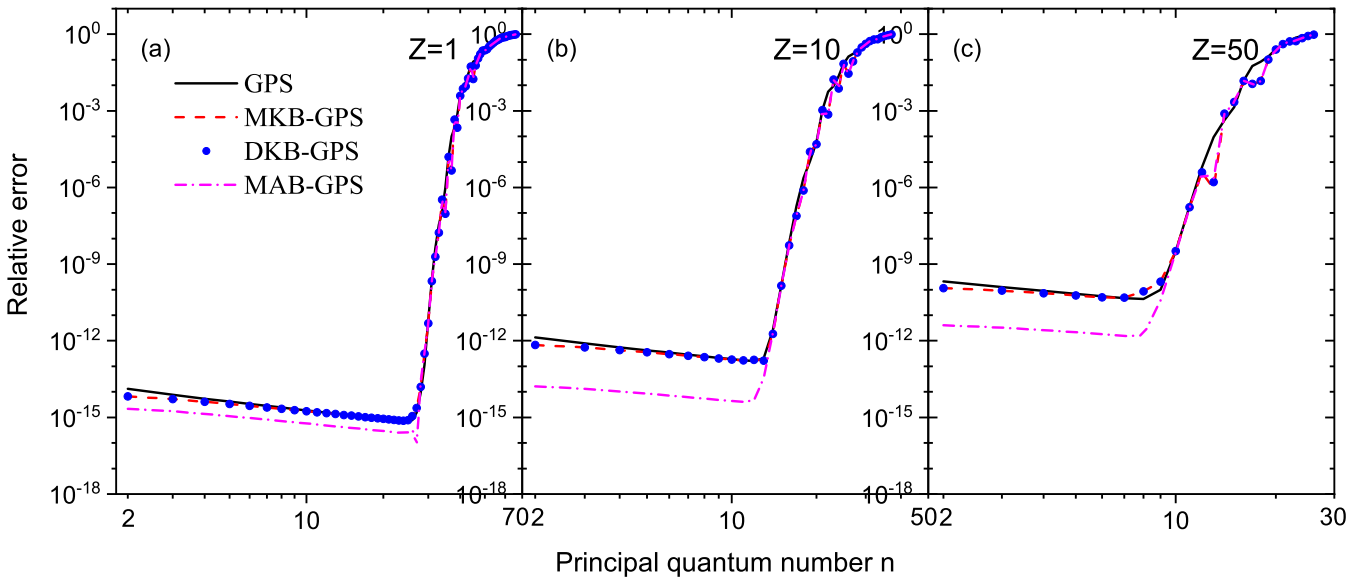

FIG. 9. Relative errors of the $p_{1/2}$ bound-state energies of the H atom and H-like ions calculated by various GPS methods with mapping parameters $N = 200$ and $k = 1$. (a) $Z = 1$ with $L = 100$, (b) $Z = 10$ with $L = 1$, and (c) $Z = 50$ with $L = 0.05$.

the electron-nucleus interaction potential is expressed in a simple analytic form:

$$V^{\mathrm{USM}}(r) = \begin{cases} -\frac{Z}{2R_0}\left(3 - \frac{r^2}{R_0^2}\right) & (r \leqslant R_0) \\ -\frac{Z}{r} & (r > R_0) \end{cases}. \tag{69}$$

The second extended nuclear model considered here is the Gaussian model (GM) where the nuclear charge is distributed in a Gaussian-type function [66]:

$$\rho^{\mathrm{GM}}(R) = Z\left(\frac{\xi}{\pi}\right)^{3/2} e^{-\xi R^2}, \tag{70}$$

in which the exponential parameter ξ is usually given by

$$\xi = \frac{3}{2\langle R^2\rangle}. \tag{71}$$

Performing the same integration as in Eq. (68), the potential $V(r)$ is found to be related to the error function

$$V^{\mathrm{GM}}(r) = -\frac{Z}{r}\mathrm{erf}(\sqrt{\xi}r). \tag{72}$$

For the H-like $^{120}Sn^{49+}$ with $Z = 50$, the root-mean-square radius of the nucleus is approximately $8.869\,44 \times 10^{-5}$ a.u. which gives the values of $R_0 \approx 1.145\,04 \times 10^{-4}$ and $\xi \approx 1.906\,77 \times 10^{8}$ in the USM and GM, respectively [66]. Figure 11(a) depicts the electron-nucleus interaction potential in the USM and GM models. The point-charge nuclear model

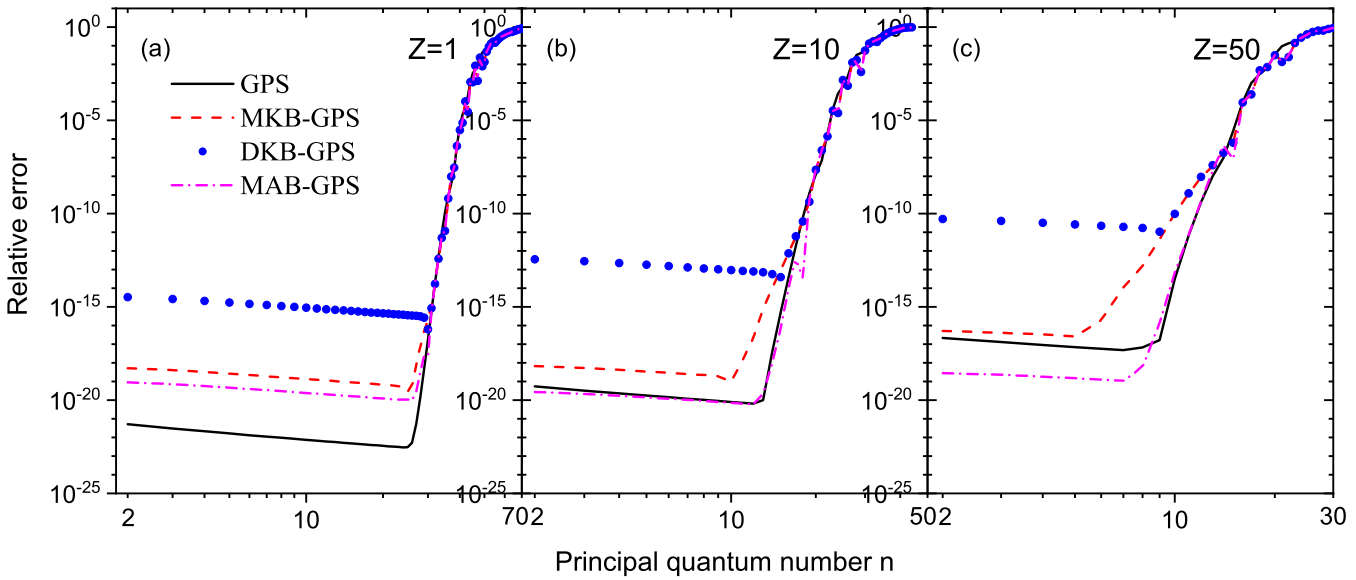

FIG. 10. Same as Fig. 9 except that $k = 2$ is used in the mapping function.

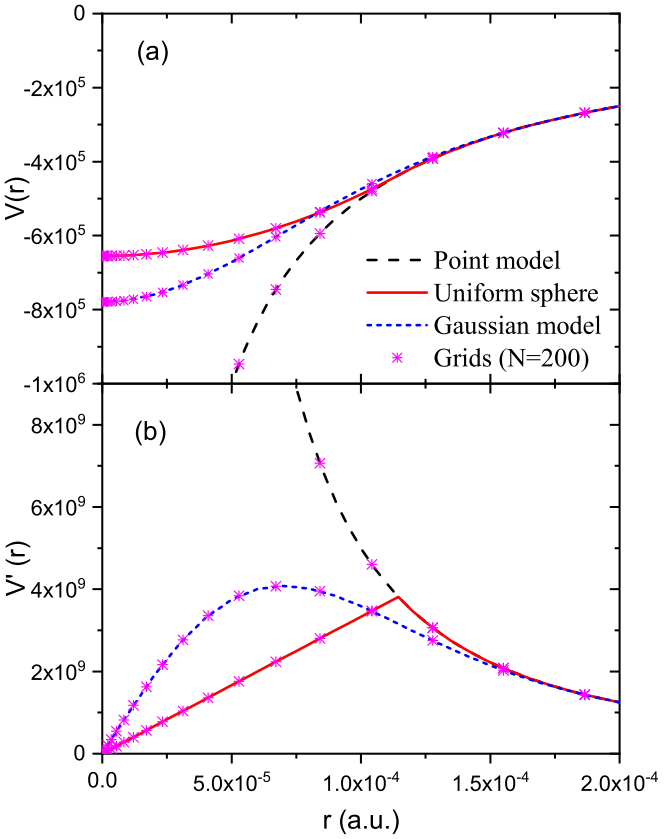

FIG. 11. The electron-nucleus interaction potentials in different nuclear models for $Z = 50$. Dots are discrete grid points used in the GPS calculations with the mapping parameters $N = 200$, $L = 0.1$, and $k = 2$. (a) The potential $V(r)$ and (b) the first-order derivative of the potential, $V'(r)$.

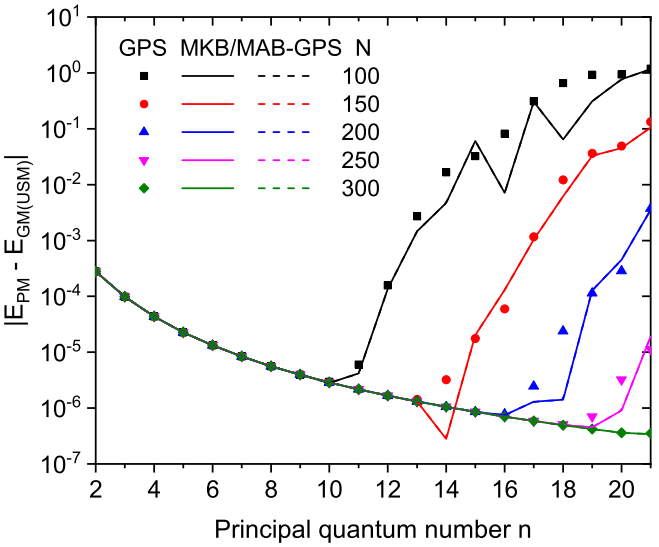

FIG. 12. Absolute differences of the energies calculated with the Gaussian-charge distribution model ($E_{\rm GM}$) and uniform-sphere model ($E_{\rm USM}$) with respect to those with point-charge nuclear model ($E_{\rm PM}$). The lowest 20 $p_{1/2}$-wave states for H-like ions with $Z = 50$ are displayed. The spurious states in the original GPS calculations have been removed. The results of MKB-GPS and MAB-GPS are indistinguishable in the figure scale. Mapping parameters of $L = 0.1$ and $k = 2$ are used in all numerical calculations for $N = 100$–300.

(PM), i.e., the exact Coulomb potential, is also included for comparison. The difference among these potentials is only visible in the small region of $r < 1.5 \times 10^{-4}$ a.u., beyond which the Coulomb interaction applies very well. Because the atomically balanced GPS methods developed here necessitate the first-order derivative of the potential $V'(r)$, its explicit form would also affect the performance of the MAB-GPS and DAB-GPS methods. Figure 11(b) displays the behavior of $V'(r)$ with the same abscissa as in Fig. 11(a). It is clear that the USM nuclear potential has a spiked peak at the nuclear boundary, i.e., a discontinuity in the second-order derivative of the potential. The GM potential, on the other hand, only depicts a smooth bump structure which further indicates that it can be well approximated by a finite-order polynomial in numerical calculations.

The finite-size effect of the nucleus on the bound-state energies is shown in Fig. 12 where the differences between the energies calculated with USM and GM potentials and those with point-charge Coulomb potential are displayed from $2p_{1/2}$ to $21p_{1/2}$ states. Four conclusions can be made from the comparison of different models using different methods.

(1) The GM and USM interaction potentials show almost the same energy shift for both low- and high-lying bound states. The magnitude of $|E_{\rm GM} - E_{\rm USM}|$ is comparably larger in lower bound states; however, it is not visible in the present figure scale.

(2) The spurious state still exists in the original GPS method; however, it would go up to a higher energy level with increasing the number of grid points. In both of our MKB-GPS and MAB-GPS calculations, the position of the spurious state is located at the third and eighth energy levels for $N = 100$ and 300, respectively. A manual removal of such state has to be done before the comparison is made.

(3) The calculations by MKB-GPS and MAB-GPS methods are indistinguishable in the figure scale. They generally follow the same trend as the original GPS method with respect to the principal quantum number n, except that they are both free of any spurious states.

(4) The convergence of all relativistic GPS methods with increasing the number of grid points N is fast. The use of a larger mapping parameter L along with a larger value of N would produce more accurate predictions on higher-lying bound states.

Although there are no analytical solutions for H-like ions with extended nuclear models, we can still get converged results by using an increasingly large number of grid points. The performance of different GPS methods at a smaller number of grid points can be estimated correspondingly, as we did in Secs. III B and III C. The energy relative errors of the $p_{1/2}$ states for the H-like ion with $Z = 50$ are displayed in Figs. 13(a), 13(b) and 13(c) for PM, GM, and USM nuclear models, respectively. All four GPS calculations are performed at $N = 200$, $L = 0.1$, and $k = 2$. The exact energies for PM are available in Eq. (9), whereas the "accurate" energies for GM and USM are produced by comparing the corresponding calculations at $N = 500$ and 600. For the point-charge model shown in Fig. 13(a), the superiority of the MAB-GPS method to the others is consistent with our conclusion made in the

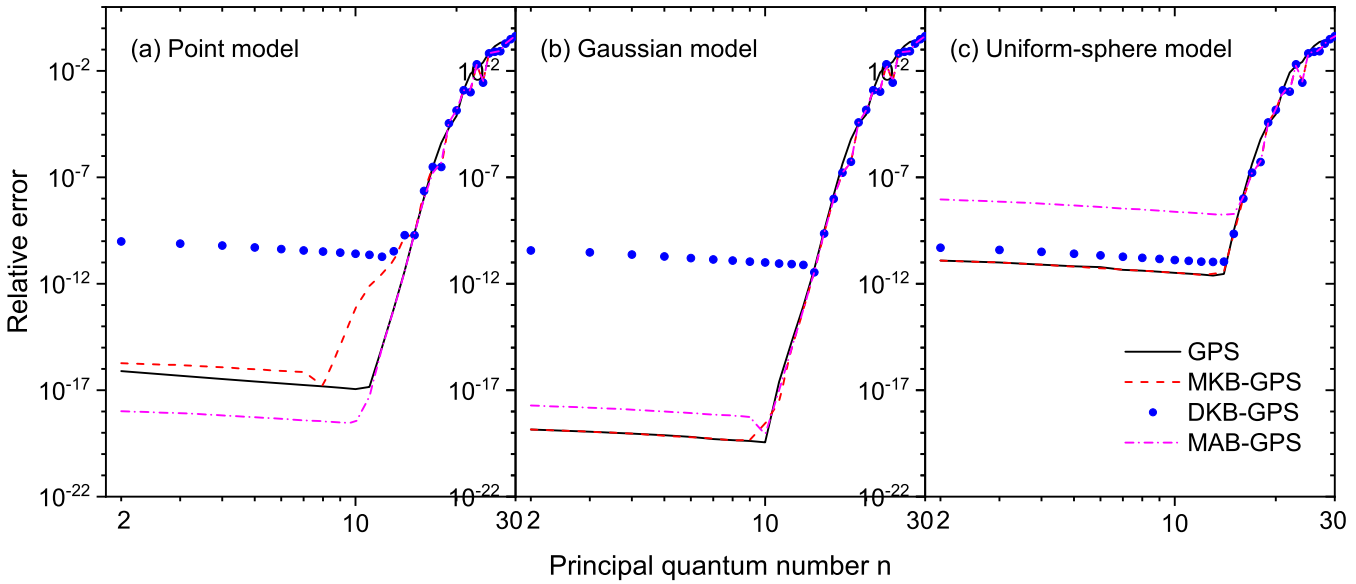

FIG. 13. Relative errors of the $p_{1/2}$ bound-state energies of the H-like ion with $Z = 50$ calculated by GPS, MKB-GPS, DKB-GPS, and MAB-GPS methods at mapping parameters $N = 200$, $L = 0.1$, and $k = 2$. The spurious states in the original GPS method are removed. (a) Point-charge nuclear model, (b) Gaussian-charge distribution model, and (c) uniform-sphere model.

previous discussion. For the Gaussian-charge distribution model, it is interestingly found that both the GPS and MKB-GPS methods improve the prediction, while the MAB-GPS method deteriorates slightly. This is understood from Eq. (B3) and Fig. 11 that the atomically balanced Hamiltonian includes the term of $V'(r)$ and the pseudospectral approximation of such a function using polynomials would introduce additional numerical errors. Compared to the calculations in the point-charge model, the accuracy of the MKB-GPS method in the Gaussian-charge model is improved by three orders of magnitude. This is attributed to the fact that in extended nuclear models, the interaction potential has no singularity at $r = 0$ and the asymptotic forms of radial wave functions for $\kappa \geqslant 1$ are [1,19]

$$P_{n\kappa}(r) \xrightarrow{r\to 0} p_1 r^{l+1}, \quad Q_{n\kappa}(r) \xrightarrow{r\to 0} q_0 r^{l}, \tag{73}$$

where p_1 and q_0 are constants. It is obvious that for the $p_{1/2}$ states investigated here, Eq. (73) manifests a faster decreasing speed than Eq. (11) as $r \to 0$, which corresponds to a better pseudospectral approximation of the radial wave functions. All the GPS calculations in the uniform-sphere nuclear model shown in Fig. 13(c) are found to be the worst in the three nuclear models. This is not surprising in consideration of the anomalous behavior of the potential at the sharp edge of the nucleus. The MAB-GPS method, which includes the additional approximation of $V'(r)$, exhibits the slowest convergence among all GPS methods. A remedy of such a problem could be accomplished by exactly placing one collocation point at the nuclear edge R_0. However, such work needs fine-tuning the mapping parameters or choosing alternative mapping functions. The relatively large errors of the DKB-GPS method do not change much in these three nuclear models and the DAB-GPS method is not stable enough in all situations. We generally conclude that, in the extended nuclear models, the MKB-GPS method probably is the best candidate for the relativistic development of the GPS method in removing the spurious states and simultaneously improving the prediction of system energies.

IV. CONCLUSION

In this paper, we have developed the mono and dual, kinetically and atomically balanced GPS methods to solve the relativistic Dirac equation without any spurious states. The robustness of these methods has been thoroughly tested with different mapping functions and for different systems in a wide variety of bound states. It has been shown that both the kinetically and atomically balanced conditions can successfully remove the spurious states with positive Dirac quantum numbers, improve the prediction of system eigenenergies, and, furthermore, amend the asymptotic behavior of radial wave functions in far distances. The dual-balanced methods do not show superiority over the mono-balanced methods in the present investigation of bound states, and their usefulness may need further exploration on physical quantities related to the negative energy states. The MAB-GPS method, which explicitly includes the interaction potential and its first-order derivative in the balanced operator, shows the best performance for systems with a point-charge nucleus. It is attributed to a better description of the singularity of the Coulomb potential at the origin. However, in the more realistic extended nuclear models where the interaction potentials do not present singularity but may have complex forms, the MKB-GPS method shows a faster convergence, a wider applicability, and an easier implementation than the others. It is therefore suggested to be the ideal candidate of the relativistic balanced GPS methods in practical investigations.

Taking advantage of the GPS method formulated in discrete variable representation, e.g., the exponential convergence of calculations with respect to the number of grid points, the simultaneously obtained system bound states in

a wide energy range, and nearly no restrictions forced upon the form of interaction potential, the relativistic balanced GPS methods developed here would provide a highly competitive tool in the high-precision calculation of few-electron atomic systems, and lay a foundation in the self-consistent Dirac-Fock, variational configuration-interaction, and relativistic density-functional calculation of more complex systems. Such applications are being developed in our group.

ACKNOWLEDGMENTS

The authors would like to thank Prof. Shih I. Chu and Prof. Dmitry A. Telnov for helpful discussions on the generalized pseudospectral method. We are also grateful to the anonymous reviewers for their very valuable and helpful suggestions that improved our manuscript substantially. Financial support from the National Natural Science Foundation of China (Grants No. 11504128, No. 11774131, and No. 91850114) is greatly acknowledged.

APPENDIX A: ATOMICALLY BALANCED CONDITION

The atomically balanced conditions enforced on the lower and upper components of the radial wave function are derived with respect to positive ($\varepsilon = E - c^2$) and negative ($\epsilon = E + c^2$) spectra, respectively. The substitution of $E = \varepsilon + c^2$ into Eq. (6) results in

$$\begin{pmatrix} V(r) & -c\left(\frac{d}{dr} - \frac{\kappa}{r}\right) \\ c\left(\frac{d}{dr} + \frac{\kappa}{r}\right) & V(r) - 2c^2 \end{pmatrix} \begin{pmatrix} P(r) \\ Q(r) \end{pmatrix} = \varepsilon \begin{pmatrix} P(r) \\ Q(r) \end{pmatrix}, \tag{A1}$$

in which the lower differential equation is

$$c\left(\frac{d}{dr} + \frac{\kappa}{r}\right) P(r) + (V(r) - 2c^2) Q(r) = \varepsilon Q(r). \tag{A2}$$

After simple algebraic manipulation, one gets

$$Q(r) = \frac{c}{2c^2 + \varepsilon - V(r)} \left(\frac{d}{dr} + \frac{\kappa}{r}\right) P(r). \tag{A3}$$

Under the assumption that $|\varepsilon| \ll 2c^2$, we have the atomic matching condition for the lower component of the radial function:

$$Q(r) = D_V^+ P(r), \tag{A4}$$

where operator D_V^+ is given by Eq. (56). If assuming further that $|V(r)| \ll c^2$, one simply has $D_V^+ \approx D^+$.

Substituting $E = \epsilon - c^2$ into Eq. (7) and utilizing the upper differential equation, one gets

$$P(r) = \frac{c}{2c^2 - \epsilon + V(r)} \left(\frac{d}{dr} - \frac{\kappa}{r}\right) Q(r). \tag{A5}$$

With the approximation $|\epsilon| \ll 2c^2$, we have the atomic matching condition for the upper component of the radial function:

$$P(r) = D_V^- Q(r), \tag{A6}$$

where D_V^- is given by Eq. (57). The assumption of $|V(r)| \ll c^2$ further simplifies $D_V^- \approx D^-$.

APPENDIX B: MAB-GPS AND DAB-GPS METHODS

The MAB-GPS method deals with a similar radial Dirac equation as Eq. (41) with the replacement of D^+ by D_V^+:

$$\begin{pmatrix} V(r) + c^2 & -c\left(\frac{d}{dr} - \frac{\kappa}{r}\right) \\ c\left(\frac{d}{dr} + \frac{\kappa}{r}\right) & V(r) - c^2 \end{pmatrix} \begin{pmatrix} 1 & 0 \\ 0 & D_V^+ \end{pmatrix} \begin{pmatrix} P'_{n\kappa}(r) \\ Q'_{n\kappa}(r) \end{pmatrix} = E \begin{pmatrix} 1 & 0 \\ 0 & D_V^+ \end{pmatrix} \begin{pmatrix} P'_{n\kappa}(r) \\ Q'_{n\kappa}(r) \end{pmatrix}. \tag{B1}$$

After mapping the variable from r to x and separating the algebraic term from the first- and second-order differential operators, one has the radial equation in the form

$$h'_D(x)\phi'(x) = E O'(x)\phi'(x), \tag{B2}$$

where

$$h'_D(x) = \begin{pmatrix} V + c^2 & \frac{\kappa(\kappa+1)}{t_-(x)f^2(x)} - \frac{V'}{t_-^2(x)c^2}\frac{\kappa}{f(x)} \\ c\frac{\kappa}{f(x)} & \frac{V-c^2}{t_-(x)c}\frac{\kappa}{f(x)} \end{pmatrix} + \begin{pmatrix} 0 & -\frac{V'}{t_-^2(x)c^2} \\ c & \frac{V-c^2}{t_-(x)c} \end{pmatrix} \frac{1}{\sqrt{f'(x)}} \frac{d}{dx} \frac{1}{\sqrt{f'(x)}} + \begin{pmatrix} 0 & -\frac{1}{t_-(x)} \\ 0 & 0 \end{pmatrix} \frac{1}{f'(x)} \frac{d^2}{dx^2} \frac{1}{f'(x)}, \tag{B3}$$

and

$$O'(x) = \begin{pmatrix} 1 & 0 \\ 0 & \frac{1}{t_-(x)c}\frac{\kappa}{f(x)} \end{pmatrix} + \begin{pmatrix} 0 & 0 \\ 0 & \frac{1}{t_-(x)c} \end{pmatrix} \frac{1}{\sqrt{f'(x)}} \frac{d}{dx} \frac{1}{\sqrt{f'(x)}}, \tag{B4}$$

in which $t_-(x)$ is defined by

$$t_-(x) = 2 - \frac{V[f(x)]}{c^2}, \tag{B5}$$

and V' represents the derivative of potential $V(r)$ with respect to r followed by a transformation of $r = f(x)$. On the assumptions of $|V(r)| \ll c^2$ as well as $|V'(r)| \ll c^2$, $t_-(x) \approx 2$ and Eqs. (B3) and (B4) are reduced to Eqs. (43) and (44), respectively.

The DAB-GPS method can be derived based on Eq. (51) with the replacements of $D^+ \to D_V^+$ and $D^- \to D_V^-$:

$$\begin{pmatrix} V(r) + c^2 & -c\left(\frac{d}{dr} - \frac{\kappa}{r}\right) \\ c\left(\frac{d}{dr} + \frac{\kappa}{r}\right) & V(r) - c^2 \end{pmatrix} \begin{pmatrix} 1 & D_V^- \\ D_V^+ & 1 \end{pmatrix} \begin{pmatrix} P''_{n\kappa}(r) \\ Q''_{n\kappa}(r) \end{pmatrix} = E \begin{pmatrix} 1 & D_V^- \\ D_V^+ & 1 \end{pmatrix} \begin{pmatrix} P''_{n\kappa}(r) \\ Q''_{n\kappa}(r) \end{pmatrix}. \tag{B6}$$

The corresponding radial equation in variable x reads

$$h_D''(x)\phi''(x) = EO''(x)\phi''(x), \tag{B7}$$

where

$$\begin{aligned} h_D''(x) &= \begin{pmatrix} V + c^2 + \frac{\kappa(\kappa+1)}{t_-(x)f^2(x)} - \frac{V'}{t_-^2(x)c^2}\frac{\kappa}{f(x)} & \frac{c}{t_+(x)}\frac{\kappa}{f(x)} \\ \frac{c}{t_-(x)}\frac{\kappa}{f(x)} & V - c^2 - \frac{\kappa(\kappa-1)}{t_+(x)f^2(x)} + \frac{V'}{t_+^2(x)c^2}\frac{\kappa}{f(x)} \end{pmatrix} \\ &+ \begin{pmatrix} -\frac{V'}{t_-^2(x)c^2} & -\frac{c}{t_+(x)} \\ \frac{c}{t_-(x)} & -\frac{V'}{t_+^2(x)c^2} \end{pmatrix} \frac{1}{\sqrt{f'(x)}}\frac{d}{dx}\frac{1}{\sqrt{f'(x)}} + \begin{pmatrix} -\frac{1}{t_-(x)} & 0 \\ 0 & \frac{1}{t_+(x)} \end{pmatrix} \frac{1}{f'(x)}\frac{d^2}{dx^2}\frac{1}{f'(x)}, \end{aligned} \tag{B8}$$

and

$$O''(x) = \begin{pmatrix} 1 & -\frac{1}{t_+(x)c}\frac{\kappa}{f(x)} \\ \frac{1}{t_-(x)c}\frac{\kappa}{f(x)} & 1 \end{pmatrix} + \begin{pmatrix} 0 & \frac{1}{t_+(x)c} \\ \frac{1}{t_-(x)c} & 0 \end{pmatrix} \frac{1}{\sqrt{f'(x)}}\frac{d}{dx}\frac{1}{\sqrt{f'(x)}}, \tag{B9}$$

in which $t_\pm(x)$ is given by

$$t_\pm(x) = 2 \pm \frac{V[f(x)]}{c^2}. \tag{B10}$$

We also note that on the assumptions of $|V(r)| \ll c^2$ as well as $|V'(r)| \ll c^2$, $t_\pm(x) \approx 2$ and Eqs. (B8) and (B9) are reduced to Eqs. (53) and (54), respectively.

One may further notice in Eqs. (B3) and (B8) that the derivative of potential V' must be explicitly provided to construct the transformed Hamiltonian. This does not cause any problems if $V(r)$ is provided in a simple and analytical form, e.g., the pure Coulomb potential or model potentials including power and exponential terms. However, when $V(r)$ is expressed in a rather complicated form such as the ambiguous fitting formula with special functions or it is only available at some discrete grid points, one may conveniently utilize the pseudospectral approximation of the first-order derivative of a function shown in Eq. (26), i.e.,

$$V' = \frac{d}{dr}V(r)|_{r=f(x)} = \frac{1}{f'(x)}\frac{d}{dx}V[f(x)], \tag{B11}$$

where

$$\frac{d}{dx}\mathcal{V}(x)|_{x=x_i} = \sum_{j=0}^{N}(d_1)_{ij}\frac{P_N(x_i)}{P_N(x_j)}\mathcal{V}(x_j). \tag{B12}$$

[1] I. P. Grant, *Relativistic Quantum Theory of Atoms and Molecules: Theory and Computation*, Springer Series on Atomic, Optical, and Plasma Physics (Springer, New York, 2006).
[2] D. H. Sampson, H. L. Zhang, and C. J. Fontes, Phys. Rep. **477**, 111 (2009).
[3] O. Zatsarinny and C. F. Fischer, Comput. Phys. Commun. **202**, 287 (2016).
[4] M. G. Kozlov, S. G. Porsev, M. S. Safronova, and I. I. Tupitsyn, Comput. Phys. Commun. **195**, 199 (2015).
[5] S. Fritzsche, Comput. Phys. Commun. **240**, 1 (2019).
[6] J. W. Braun, Q. Su, and R. Grobe, Phys. Rev. A **59**, 604 (1999).
[7] C. J. Joachain, M. Dorr, and N. J. Kylstra, Adv. At. Mol. Opt. Phys. **42**, 225 (2000).
[8] F. Krausz and M. Ivanov, Rev. Mod. Phys. **81**, 163 (2009).
[9] X. Antoine and E. Lorin, J. Comput. Phys. **395**, 583 (2019).
[10] S. Selstø, E. Lindroth, and J. Bengtsson, Phys. Rev. A **79**, 043418 (2009).
[11] M. Lewin and É. Séré, Proc. London Math. Soc. **100**, 864 (2010).
[12] I. I. Tupitsyn and V. M. Shabaev, Opt. Spectrosc. **105**, 183 (2008).
[13] V. M. Shabaev, I. I. Tupitsyn, V. A. Yerokhin, G. Plunien, and G. Soff, Phys. Rev. Lett. **93**, 130405 (2004).
[14] K. Beloy and A. Derevianko, Comput. Phys. Commun. **179**, 310 (2008).
[15] C. F. Fischer and O. Zatsarinny, Comput. Phys. Commun. **180**, 879 (2009).
[16] G. W. F. Drake and S. P. Goldman, Phys. Rev. A **23**, 2093 (1981).
[17] H. M. Quiney, I. P. Grant, and S. Wilson, J. Phys. B **22**, L15 (1989).
[18] I. P. Grant and H. M. Quiney, Phys. Rev. A **62**, 022508 (2000).
[19] I. P. Grant, *Springer Handbook of Atomic, Molecular, and Optical Physics* (Springer, New York, 2006).
[20] C. F. Fischer, G. Gaigalas, P. Jönsson, and J. Bieroń, Comput. Phys. Commun. **237**, 184 (2019).
[21] W. R. Johnson, S. A. Blundell, and J. Sapirstein, Phys. Rev. A **37**, 307 (1988).
[22] J. Sapirstein and W. R. Johnson, J. Phys. B **29**, 5213 (1996).
[23] L. Y. Tang, Y. H. Zhang, X. Z. Zhang, J. Jiang, and J. Mitroy, Phys. Rev. A **86**, 012505 (2012).
[24] A. Igarashi, J. Phys. Soc. Jpn. **76**, 054301 (2007).
[25] I. P. Grant, J. Phys. B **42**, 055002 (2009).
[26] S. Salomonson and P. Öster, Phys. Rev. A **40**, 5548 (1989).
[27] J. Y. Fang, S. W. Chen, and T. H. Heng, Nucl. Sci. Tech. **31**, 15 (2020).
[28] T. C. Scott, J. Shertzer, and R. A. Moore, Phys. Rev. A **45**, 4393 (1992).
[29] H. Almanasreh, S. Salomonson, and N. Svanstedt, J. Comput. Phys. **236**, 426 (2013).
[30] H. Almanasreh, J. Comput. Phys. **376**, 1199 (2019).
[31] E. Layton and Shih-I Chu, Chem. Phys. Lett. **186**, 100 (1991).

[32] E. Ackad and M. Horbatsch, J. Phys. A: Math. Gen. **38**, 3157 (2005).
[33] D. Baye, L. Filippin, and M. Godefroid, Phys. Rev. E **89**, 043305 (2014).
[34] D. Baye, Phys. Rep. **565**, 1 (2015).
[35] C. Canuto, M. Y. Hussaini, A. Quarteroni, and T. A. Zang, *Spectral Methods: Fundamentals in Single Domains* (Springer-Verlag, Berlin, 2006).
[36] A. Deloff, Ann. Phys. (NY) **322**, 1373 (2007).
[37] G. Yao and Shih-I Chu, Chem. Phys. Lett. **204**, 381 (1993).
[38] X. M. Tong and Shih-I Chu, Chem. Phys. **217**, 119 (1997).
[39] Shih-I Chu and D. A. Telnov, Phys. Rep. **390**, 1 (2004).
[40] Shih-I Chu and D. A. Telnov, J. Chem. Phys. **123**, 062207 (2005).
[41] D. A. Telnov and Shih-I Chu, Phys. Rev. A **80**, 043412 (2009).
[42] D. A. Telnov and Shih-I Chu, Comput. Phys. Commun. **182**, 18 (2011).
[43] A. K. Roy, Int. J. Quantum Chem. **113**, 1503 (2013).
[44] A. K. Roy, Int. J. Quantum Chem. **115**, 937 (2015).
[45] A. K. Roy, Int. J. Quantum Chem. **116**, 953 (2016).
[46] L. Zhu, Y. Y. He, L. G. Jiao, Y. C. Wang, and Y. K. Ho, Phys. Plasmas **27**, 072101 (2020).
[47] L. Zhu, Y. Y. He, L. G. Jiao, Y. C. Wang, and Y. K. Ho, Int. J. Quantum Chem. **120**, e26245 (2020).
[48] Y. Y. He, L. G. Jiao, A. Liu, Y. Z. Zhang, and Y. K. Ho, Eur. Phys. J. D **75**, 126 (2021).
[49] L. G. Jiao, Y. Y. He, Y. Z. Zhang, and Y. K. Ho, J. Phys. B **54**, 065005 (2021).
[50] D. A. Telnov and Shih-I Chu, Phys. Rev. A **59**, 2864 (1999).
[51] A. K. Roy and Shih-I Chu, Phys. Rev. A **65**, 052508 (2002).
[52] Z. Zhou and Shih-I Chu, Phys. Rev. A **71**, 022513 (2005).
[53] A. K. Roy, J. Phys. B **38**, 1591 (2005).
[54] J. Heslar and Shih-I Chu, Phys. Rev. A **86**, 032506 (2012).
[55] D. A. Telnov, D. A. Krapivin, J. Heslar, and Shih-I Chu, J. Phys. Chem. A **122**, 8026 (2018).
[56] D. A. Telnov and Shih-I Chu, Phys. Rev. A **102**, 063109 (2020).
[57] E. Tiesinga, P. J. Mohr, D. B. Newell, and B. N. Taylor, The 2018 CODATA recommended values of the fundamental physical constants (web version 8.1), database developed by J. Baker, M. Douma, and S. Kotochigova, available at http://physics.nist.gov/constants, National Institute of Standards and Technology, Gaithersburg, MD, 2020.
[58] H. A. Bethe and E. E. Salpeter, *Quantum Mechanics of One- and Two-Electron Atoms* (Dover, New York, 2008).
[59] Equations (18) and (20) in Ref. [37] may contain typos in the derivation of the Hamiltonian matrix.
[60] D. A. Telnov, K. E. Sosnova, E. Rozenbaum, and Shih-I Chu, Phys. Rev. A **87**, 053406 (2013).
[61] L. Visscher, P. J. C. Aerts, O. Visser, and W. C. Nieuwpoort, Int. J. Quantum Chem. **40**, 131 (1991).
[62] M. G. Kozlov and I. I. Tupitsyn, Atoms **7**, 92 (2019).
[63] F. Fillion-Gourdeau, E. Lorin, and A. D. Bandrauk, J. Comput. Phys. **307**, 122 (2016).
[64] The spurious states shown in the figure calculated by the GPS method do not increase exponentially as r goes to infinity, and this is due simply to the fact that the grid points are too sparse in the far asymptotic region.
[65] J. P. Desclaux, At. Data Nucl. Data Tables **12**, 311 (1973).
[66] L. Visscher and K. G. Dyall, At. Data Nucl. Data Tables **67**, 207 (1997).